Contents lists available at ScienceDirect

Process Safety and Environmental Protection

journal homepage: www.journals.elsevier.com/process-safety-and-environmental-protection

Performance assessment of standalone hydrogen water electrolyzer production system based on waste heat power generation and humidification dehumidification system

M.A. Mahmoud [a,b], Sameh Nada [a,b], Shinsuke Mori [a,c], Hamdy Hassan [a,d,*]

[a] Department of Energy Resources Engineering, Egypt-Japan University of Science and Technology, Alexandria 21934, Egypt
[b] Department of Mechanical Engineering, Benha Faculty of Engineering, Benha University, Benha, Egypt
[c] Department of Chemical Science and Engineering, Tokyo Institute of Technology, Tokyo 152-8550, Japan
[d] Mechanical Power Engineering Department, Faculty of Engineering, Assiut University, Assiut 71516, Egypt

ARTICLE INFO

Keywords:
Waste heat recovery
Standalone system
Saturated steam
Thermoelectric generators
Humidification dehumidification
Hydrogen production

ABSTRACT

This study evaluates the performance of a new standalone integrated system for independent hydrogen production combining waste heat recovery (WHR) via thermoelectric generators, humidification-dehumidification (HDH), and a proton exchange membrane (PEM) electrolyzer. The system's behavior is analyzed at varying steam inlet temperatures and qualities to identify the best configuration for power generation. A complete mathematical model of the whole system unit is constructed, programmed inside Matlab, solved, and validated. Four configurations are studied for the thermoelectric generator unit distributions [100×100], [50×200], [25×400], and [12×833]. Configuration 4 (12×833 TEG arrangement) outperforms others, generating 36.88 kW at 160 °C and 0.97 steam inlet quality, a 130 % increase compared to 100 °C. This configuration extracts 337 kW from steam, enabling a hydrogen production rate of 15.5 kg/day with PEM efficiency peaking at 73.65 % (declining to 68.94 % at 160°C due to overpotentials). The HDH unit is operating at a GOR of 1.892. The system efficiency increased from 4.45 % at 100°C to 4.95 % at 160 °C, driven by enhanced TEG power generation. Economic analysis reveals a levelized hydrogen cost (LCOH) of 2.22–2.22–2.96/kg, competitive with blue hydrogen markets. Net Present Value (NPV) analysis shows profitability at 3–5 $/kg hydrogen, with breakeven at 10–20 years for 3 $/kg and 4–5 years for 5 $/kg. Excess water utilization in the PEM electrolyzer reaches near-zero at 160°C, contrasting with 55 % excess at 100°C. Trade-offs between steam quality and hydrogen yield are quantified: increasing quality from 0.05 to 0.97 at 100°C raises hydrogen production by 0.45 % (6.97–7.01 kg/day), while higher temperatures prioritize power over electrolyzer efficiency.

1. Introduction

The global energy sector accounts for 73 % of anthropogenic greenhouse gas emissions("Energy Systems," 2023), necessitating rapid decarbonization. As a versatile, high-energy-density (120–142 MJ/kg, 33 kWh/kg) fuel with zero direct CO_2 emissions, hydrogen is pivotal for hard-to-abate sectors like heavy industry and long-haul transport. However, 95 % of global hydrogen production remains fossil fuel-dependent ("gray" hydrogen), emitting 9–12 kg CO_2 per kg H_2 (Giakoumakis and Sidiras, 2025). Transitioning to low-carbon 'green' hydrogen—produced via water electrolysis using renewable electricity—is critical and becoming economically viable, with levelized costs estimated at approximately €3.23/kg in 2019, though broader challenges like resource constraints remain relevant (Glenk and Reichelstein, 2019)

These merits encouraged researchers to discover different methods and develop innovative technologies for hydrogen generation (Nasser et al., 2022a). The advantage of hydrogen production is its versatility in terms of energy sources (Dincer and Acar, 2014).

In the generation process, electrical power input is vital for water electrolysis. This input power facilitated the splitting of water molecules into hydrogen and oxygen atoms. The splitting process depends on the energy input. Electrolysis technologies like proton exchange membranes (PEM) and solid oxide electrolysis cells (SOECs) offer pathways to green hydrogen. PEM electrolyzers, operating at 50–80°C, achieve efficiencies of 60–75 % but require ultrapure water and 4.8–5.4 kWh/m^3 electricity (Shiva Kumar and Lim, 2022; Wang et al., 2021). SOECs, while more

* Corresponding author at: Department of Energy Resources Engineering, Egypt-Japan University of Science and Technology, Alexandria 21934, Egypt.
E-mail addresses: hamdyaboali@yahoo.com, hamdy.aboali@ejust.edu.eg (H. Hassan).

https://doi.org/10.1016/j.psep.2025.107364
Received 2 February 2025; Received in revised form 25 April 2025; Accepted 23 May 2025

Nomenclature

Latin Symbol .

Symbol	DescriptionUnit
A	Aream^2
Cp	Specific heatJ·kg^{-1} ·K^{-1}
Dh	Hydraulic diameterm
E	Electrical energykW
F	Faraday constantC·mol^{-1}
Gm	Mass velocitykg·m^{-1} ·s^{-1}
H	EnthalpykJ·kg^{-1}
h_{fg}	Latent heat of vaporizationJ·kg^{-1}
I	Generated currentA
J	Current densityA·cm^{-2}
K	Thermal conductivityW·m^{-1} ·K^{-1}
L	Lengthm
$\dot{m}$	Mass flow ratekg·s^{-1}
N	Polytropic index—
$\dot{N}$	Molar flow ratemol·s^{-1}
Nu	Nusselt number—
Pr	Prandtl number—
Pr	Reduced pressure—
Q	Heat transfer rateW
R	Electrical resistanceΩ
R''_{tc}	Solid/solid thermal resistanceK·W^{-1}
rp_{stage}	Pressure ratio per compressor stage—
RH	Relative humidity%
T	TemperatureK
V	VoltageV
W_{stage}	Work done by each compressor stageW
X	Salt concentration or steam qualityppm or —

Greek Symbols .

Symbol	DescriptionUnit
η	Efficiency—
λ(x)	Water content at location *x*—
σ	Local ionic conductivityS·m^{-1}
ω	Air-specific humiditykg vapor·kg^{-1} dry air
ρ	Electrical resistivityΩ·m
α	Seebeck coefficientV·K^{-1}

Abbrivation and substracts .

Term	Description
CA	Closed Air
CAOW	Closed Air, Open Water
CW	Closed Water
CWOA	Closed Water, Open Air
comp	Compressor
Conv	Convection
eff	Effective
GOR	Gained Output Ratio
HDH	Humidification-Dehumidification
HHV	Higher Heating Value
HX	Heat Exchanger
MEE	Multi-Effect Evaporation
MSF	Multi-Stage Flash
ORC	Organic Rankine Cycle
PEM	Proton Exchange Membrane Electrolyzer
PV	Photovoltaic
RO	Reverse Osmosis
RR	Recovery Ratio
SOEC	Solid Oxide Electrolysis Cells
sw	Seawater
TEG	Thermoelectric Generator
WHR	Waste Heat Recovery
a	Ambient / Anode
c	Cold / Cathode
h	Hot
pn	Positive / Negative leg

efficient (>85 %) at 600–1000°C, face material degradation challenges and higher capital costs(Zarabi Golkhatmi et al., 2022). Both technologies underscore a critical bottleneck: the energy-water nexus. A significant volume of residual thermal energy is discharged into the atmosphere by various industrial processes presents a valuable opportunity for power generation. This waste heat, often available at grades (low, medium, and high) ↱↱(bchoate) presents an underutilized solution. Industrial processes discard 20–50 % of energy input as low-grade heat (<250°C) (Ononogbo et al., 2023). These WHR systems are compatible with power stations for producing the necessary input electricity for water electrolysis (Khater et al., 2021). To mitigate the energy consumption challenges associated with hydrogen production, this study investigated the integration of WHR systems. New techniques are emerging to generate electricity from waste heat directly. TEGs are a promising avenue for transforming low-grade waste heat into electricity, which can subsequently be employed as power electrolyzers for hydrogen generation. The thermoelectric generators (TEGs) can convert into electricity via the Seebeck effect ↱↱(Olabi et al., 2022). TEGs are especially attractive for harnessing low-grade waste heat owing to their advantages of simplicity and adaptability and not require moving parts (solid-state) or working fluids such as traditional power. Incorporating TEG technology into WHR systems allows for recovering waste heat from different sources and converting it into usable electricity, reducing the use of fossil fuels and decreasing the amount of CO_2 emissions to the atmosphere (Hewawasam et al., 2020; Jouhara et al., 2017). TEG technology has a lower current conversion efficiency of around 4–7 %, TEGs excel in utilizing what would otherwise be wasted heat, making them a cost-effective solution (Rowe and Min, 1998; Yang et al., 2017).

TEGs utilize the Seebeck effect to directly convert the temperature difference between two points (Rowe and Bhandari, 1983). These devices include abundant pairs of positive and negative types of semiconductor materials arranged in a specific manner to maximize voltage generation. By creating a temperature difference across these materials, TEGs can produce usable electrical power. Several systematic models have been suggested to enhance the efficiency of WHR systems utilizing TEG modules while optimizing TEG performance requires rigorous modeling approaches that consider specific application details. Studying the dynamics of fluids and adjusting operating conditions can significantly influence the direct conversion of waste heat into electricity (Hsiao et al., 2010; Ma et al., 2015). Many studies have explored different methods to enhance the performance of TEG systems. For Example, the temperature of the fluid inlet to the system, flow rate, thermal and electrical resistance in contact, fluid flow properties, and design of heat exchangers can be changed.

Studies conducted by ↱(Niu et al., 2009) suggested that increasing inlet temperatures and optimizing flow rates of the hot fluid stream can substantially enhance the electricity produced from the TEGs system. Sasaki et al. (Sasaki et al., 2014) presented the TEG systems with more than 2500 modules and operated this TEG system utilizing spring water as an energy source with temperatures around 82 and 96 °C. In another study by Ahiska et al. (Ahiska and Mamur, 2013) increasing the flow rate for both hot and cold fluids led to higher power output and a more significant temperature differential across the TEG. The design of the heat exchanger (HX) has a significant effect on TEG performance. Lesage et al. (2013) examined different HX designs and found that a slotted flat HX design generates the highest power output, despite having higher flow resistance. Rezania et al. (2012) embedded microchannel HX into TEG systems, leading to a significant improvement in net output power. Material selection also plays a role.

Generating electricity from waste heat is crucial, but having water available for the electrolysis process is just as important. This study investigates the use of the HDH unit to produce the required water by utilizing the waste heat from the system to drive the process. A small-scale humidification-dehumidification desalination technology can generate 1/300 m^3/day of distillate water. This is a major advantage of HDH units over other desalination systems such as RO, MSF, and MEE. Another advantage of HDH units is their ability to utilize low-grade temperature energy sources for water heating. Additionally, they can effectively treat water with salinity levels far exceeding seawater (>35,000 ppm). Finally, HDH units require lower maintenance than other desalination technologies (Dave and Krishnan, 2021; G. Prakash Narayan et al., 2010). The HDH system is comprised of an evaporator (humidifier), condenser (dehumidifier), heater (heat exchanger), and an air stream. The air stream acts as a carrier, transferring water vapor from the humidifier bed to the dehumidifier. A heater or heat exchanger is employed to add thermal energy to feed water before its introduction into the humidifier. HDH technology systems can be classified based on the type of heating used, such as water-heated systems or air-heated systems(Garg et al., 2018). The cycle type can be either a CAOW or a CWOA. Narayan et al. (G Prakash Narayan et al., 2010) conducted a comprehensive thermodynamic analysis of various HDH cycle configurations. The HDH performance was assessed based on the GOR under diverse inlet conditions. This study revealed that the CW and CA cycles demonstrate comparable thermodynamic performance, although the efficiency of traditional water-heated cycles is significantly impacted by dehumidifier performance. Prakash Narayan et al. (2010) concluded that the CAOW and water-heated humidification-dehumidification cycles generally outperform the CWOA cycle. This is because, in the CWOA cycle, the humidification process may not adequately cool the water, leading to a higher coolant temperature at the dehumidifier inlet. This limitation can negatively impact water production rates due to the reduced capacity of the humid air compared to open water cycles.

Recent studies have further underscored hydrogen's central role in sustainable energy transitions. For example, (Noor and Amin, 2024) provided a thorough overview of hydrogen's potential in coupling with solar, wind, and hybrid systems. It emphasized hydrogen as an energy vector capable of seasonal storage and sectoral coupling, promoting grid resilience and decarbonization. Similarly, (Ding et al., 2025) proposed an advanced configuration incorporating multi-level waste heat utilization, with PEM electrolysis to produce hydrogen sustainably, supported by energy, exergy, environmental, and economic (4E) analyses. Moreover, (Nurizat Rahman and Abdul Wahid, 2024) assessed green hydrogen viability under uncertain energy prices, identifying policy interventions and location-specific configurations that improve cost-competitiveness and reduce risk.

Despite significant advancements in waste heat recovery (WHR), humidification-dehumidification (HDH) desalination, and proton exchange membrane (PEM) electrolysis, existing studies have yet to integrate these technologies into a unified, energy-efficient system capable of maximizing waste heat valorization. While these components have been explored individually or in paired configurations, no prior work has combined thermoelectric generators (TEGs), HDH desalination, and PEM electrolysis into a self-sustaining system powered exclusively by low-grade waste steam (water-vapor mixture) (100–160 °C, 0.05–0.97 quality). Additionally, the potential to reutilize the exhaust water vapor mixture from the TEG WHR system

in a dual-loop process: (1) preheating seawater for HDH desalination and (2) reheating freshwater to 353 K for PEM electrolysis, minimizing thermal losses. So, in this study, the performance of a standalone waste steam heat recovery system for hydrogen production is investigated. The system is composed of thermoelectric generators for power generation by maximizing latent heat extraction, and a humidification dehumidification unit for freshwater production to run the electrolyzer investigated. A complete mathematical model is constructed, programmed, and solved inside Matlab and validated. The study is investigated for four configurations of the TEGs units distributions in the direction of the waste steam flow: 1[100×100], **2**[50×200], **3** [25×400], and 4 [12×833]. The system's performance is evaluated under varying parameters, including steam inlet quality, steam mass flow rate, and steam inlet temperatures. The exhaust steam from the TEGs is leveraged in a two-step process. First, it preheats seawater in the HDH desalination process, enhancing the evaporation and condensation cycles. Next, it is utilized in a final heat exchanger to reheat freshwater, optimizing its temperature for the PEM electrolysis process. This dual-use strategy ensures minimal thermal energy loss while improving system efficiency. Moreover, the study incorporates an economic assessment through the Levelized Cost of Hydrogen (LCOH) and Net Present Value (NPV) analysis. These metrics are used to evaluate the financial feasibility of the proposed system and benchmark it against conventional and emerging hydrogen production pathways. The novelty of this research lies in its integration of WHR, HDH desalination, and PEM electrolysis into a self-sustaining, standalone system. This system not only enlarges waste heat conversion into electricity but also strategically repurposes thermal energy to enhance the desalination and hydrogen production processes. This system capability makes it highly suitable for off-grid or remote applications, offering a robust solution for decentralized energy and water needs.

2. Physical model description

The system illustrated in Fig. 1 comprises several integrated units: a WHR system, an HDH unit, and a hydrogen production unit. This innovative system integrates multiple technologies to maximize resource utilization and promote sustainability. By combining waste heat recovery, water desalination, and hydrogen production, it offers a potential solution for addressing energy, water scarcity, and clean fuel challenges simultaneously. Such integrated approaches may significantly contribute to the development of more efficient and environmentally sustainable industrial processes. The WHR unit employs TEG modules to capture latent heat from a waste heat source (saturated steam) at state (i), converting it into electrical energy. Residual heat exits the WHR system at state (h) and is transferred to a heat exchanger in the HDH unit. In the desalination unit, the remaining thermal heat is utilized to elevate the temperature of water in a counter-flow heat exchanger, with the water entering at state (2) and exiting at state (3) before being sprayed onto a humidified bed. The air stream within the HDH unit absorbs water vapor from the humidifier and then passes through a coil where the vapor condenses into fresh water, which is collected in a tank at state (5). The saltwater, having passed through the humidifier, exits at state (4). Finally, the freshwater is directed to a heater (heat exchanger) to increase its temperature to state (9), after which it enters a PEM electrolyzer for hydrogen production. The PEM electrolyzer uses the thermal energy stream exit from the HDH unit at state (p) to reheat fresh water after the splitting process a process called electrolysis, and the thermal energy steam finally exits at condition (O). The produced hydrogen is then collected and stored for various applications, such as fuel cells or industrial processes. Meanwhile, depending on the system's design and requirements, the oxygen byproduct can be vented into the atmosphere or captured for other uses.

2.1. Waste heat recovery system (WHR)

As shown in Fig. 1, the WHR system is designed to harness thermal energy from low-grade waste heat as a water vapor mixture. This steam is extracted from the exhaust of a back-pressure industrial steam turbine (SST-600 module), commonly implemented in steam power plants. The turbine allows condensation at saturated pressures, corresponding to saturation temperatures. This exhaust steam represents a viable low-

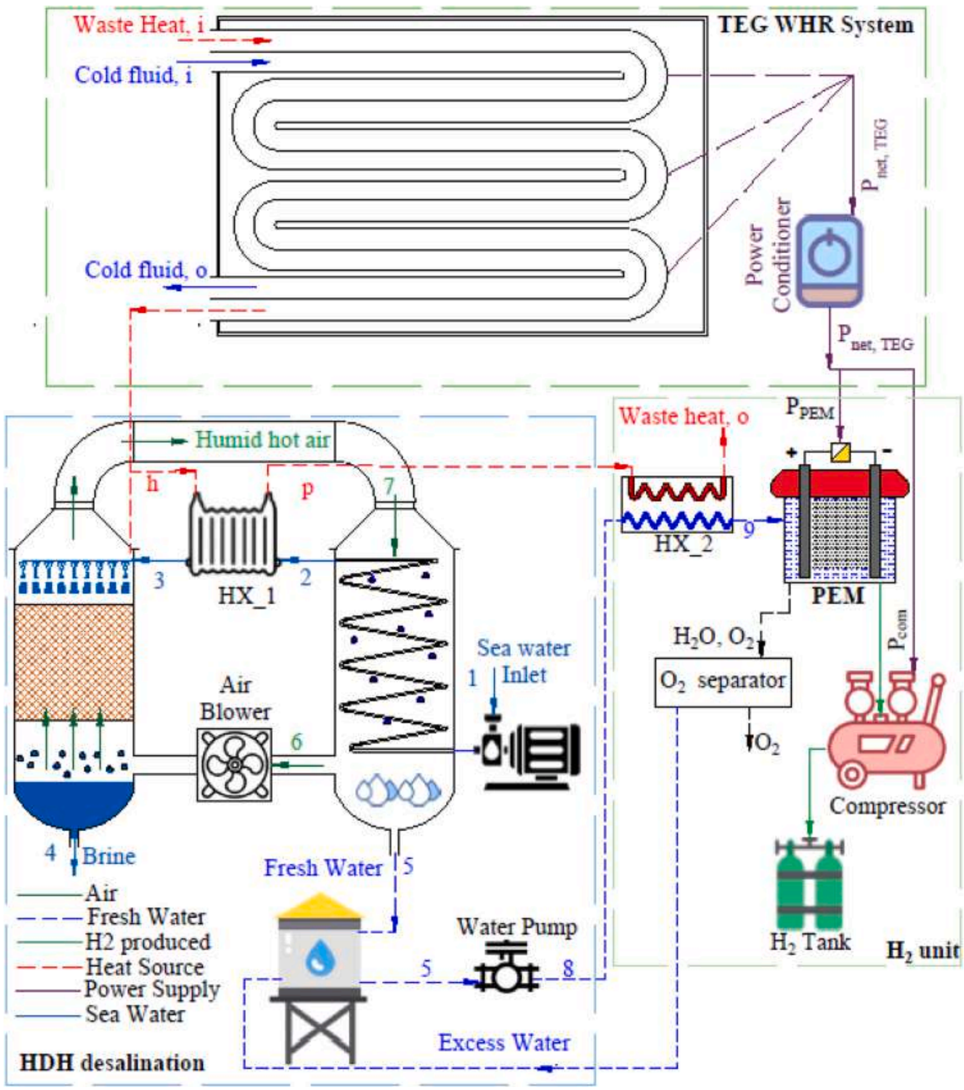

Fig. 1. The system integrates a WHR unit, HDH unit, and a hydrogen production unit.

grade heat source for thermoelectric power generation.

The configuration supports a cascaded use of energy — first in thermoelectric generation, then in thermal desalination, and finally in PEM electrolysis. This layered utilization enhances overall system sustainability. The layout in Fig. 1, therefore, serves not only as a schematic but as a conceptual map of energy flow and integration within the proposed standalone hydrogen production system. The WHR system includes a parallel-flow heat exchanger fitted with thermoelectric generator (TEG) modules arranged to maximize heat transfer from the steam to the TEG surfaces. To assess the maximum power generation capability, four distinct configurations of TEG module arrangements were analyzed: 100 modules arranged in 100 rows (100 ×100), 50 rows of 200 modules (50 ×200), 25 rows of 400 modules (25 ×400), and 12 rows of 833 modules (12 ×833), as illustrated in Fig. 2. These configurations are strategically positioned to enhance thermal contact and optimize heat extraction. On both sides of each TEG module, high thermal conductivity aluminum heat sinks with a plate-fin design are employed, as shown in Fig. 3. These heat sinks improve the heat transfer rate and help maintain the temperature gradient across the TEG surfaces, thus maximizing electrical output. Geometrical dimensions of the heat sinks, which play a critical role in system performance, are provided in Table 1.

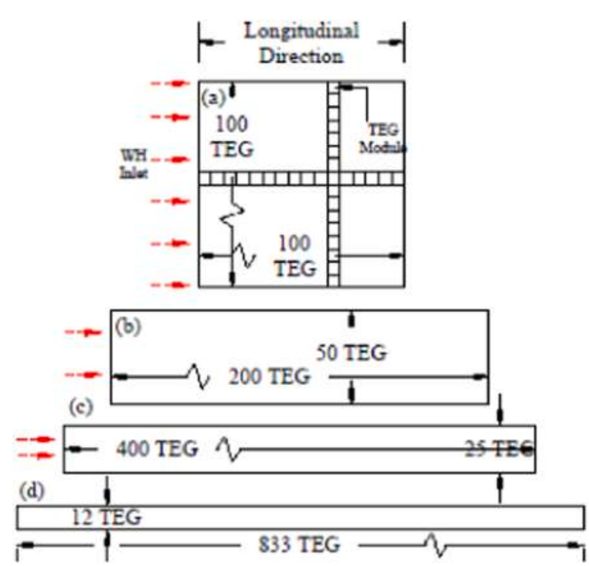

Fig. 2. Different Configurations Arrangement **(a)** Configuration- 1 [100 × 100], **(b)** [50 × 200], **(c)** [25 × 400], and **(d)** Configuration- 4 [12 × 833].

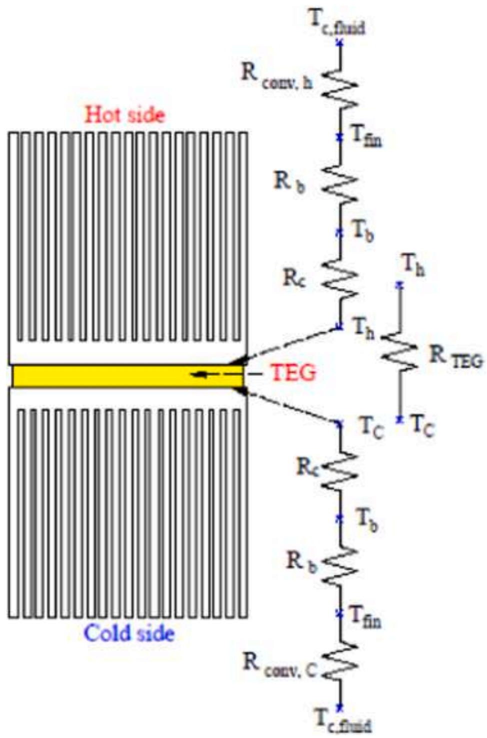

Fig. 3. Thermal resistance model for TEG Module.

2.2. Humidification-dehumidification unit (HDH)

In this study, a CAOW and water-heated HDH unit are selected based on previous research findings (G. Prakash Narayan et al., 2010) as shown in Fig. 4. CAOW systems generally outperform CWOA systems because increasing the water temperature at the dehumidifier inlet can negatively affect freshwater production due to a decrease in the capacity of humid air that can condense on the dehumidifier coils compared to open water cycles. One of the main parts of the HDH unit is the packed-bed humidifier, as shown in Fig. 1. This component seems like a counter-flow heat and mass exchanger. Air enters the humidifier at condition (6) and absorbs water vapor through an evaporative process as it passes through the packed bed layers. The air exits the humidifier at point (7), with a higher humidity level than at the inlet. There is an important relationship between the seawater inlet flow rate and the humidifier cross-sectional area (water flux). The ratio between seawater flow rate (at state point 3) and humidifier cross-sectional area is typically in the range of 0.8–4.0 kg/sec·m^2 (Sharqawy et al., 2014). Another component of the HDH unit is the dehumidifier (condenser), as depicted in Fig. 5. This part is responsible for condensing the vapor present in the moist hot air that enters the dehumidifier at state point 7. Sea water passes through the tubes within the dehumidifier at a specific temperature and mass flow rate. At the same time, the air at state (7) flows along the plate fins, making water vapor droplets condense and fall due to gravity. The condenser section employs plate fins to raise the air side surface area, thereby enhancing heat transfer between the saltwater inside the tubes and the humid air flowing over them (Sievers and Lienhard V., 2015). The counter-flow heat exchanger displayed in Fig. 1, acts as a connecting component between the humidifier and dehumidifier sections. This heat exchanger is responsible for heating the preheated seawater inlet, raising its temperature from state point 2 to state point 3, also known as the top brine temperature. The heating process is facilitated by utilizing the waste heat stream exiting the WHR system at the identified state point (h).

2.3. Hydrogen production unit

The WHR unit employs TEG modules to capture latent heat from a water vapor mixture source, converting it into electricity. This recovered energy is then used to operate PEM electrolyzer for producing hydrogen. The hydrogen cycle, depicted in Fig. 1, primarily consists of a PEM electrolyzer, a water tank, a water pump, and a heat exchanger (HX-2). The water used in the electrolysis process is generated by the HDH unit. The water pump circulates the water at the required pressure level for the PEM, while the heat exchanger raises the water temperature to the desired level before it enters the electrolyzer. The electrolysis process involves using heated water (state point 9). Electrochemical reactions driven by electricity were employed to split water into oxygen and hydrogen. Hydrogen was generated at the cathode, while oxygen was generated at the anode.

3. Thermodynamic modeling

Thermodynamic modeling is developed and validated to gain a deeper understanding of the hybrid system's performance. This section investigates electrochemical and thermodynamic analysis. To make it more comprehensible, the following premises are accepted. The system is assumed to operate under steady-state conditions. Pressure variations within the system are considered minimal. The impact of kinetic and potential energy is assumed to be neglected. Heat losses from the system's components are proposed to be minimal. All needed inputs for modeling are recorded in Table 2.

Table 1
Gematrical dimensions of the aluminium plate-fin heat sink ↱(Pujol et al., 2023).

Parameter	Variable	Units	Value
Width	W	mm	41
length	L	mm	40.5
Fin height	L_{fin}	mm	36
Fin width	W_{fin}	mm	41
Fin thickness	t_{fin}	mm	1.3
Fin- to- fin distance	d	mm	0.9
Number of fins	n		19
Thermal conductivity	K_{fin}	W/m. k	235
Base height	L_b	mm	4

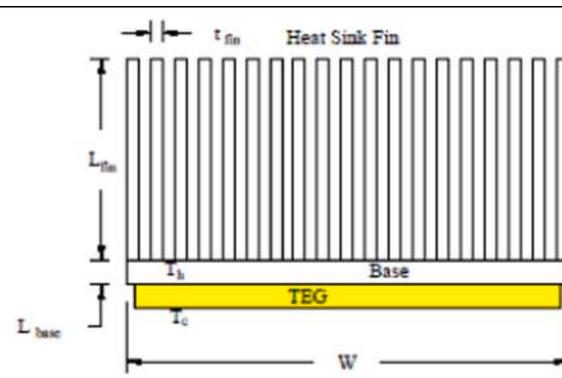

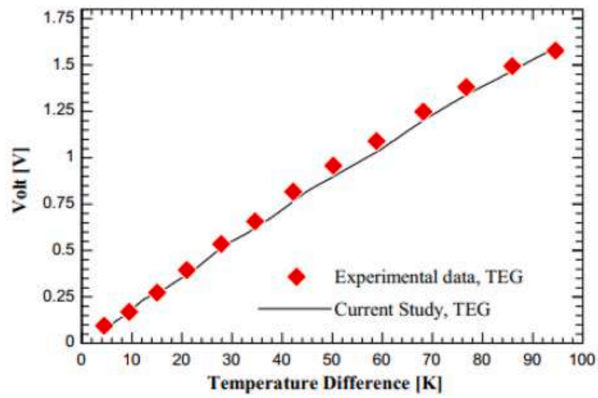

(a) Numerical and experimental results (Khalil and Hassan, 2019) for the TEG module in the WHR system.

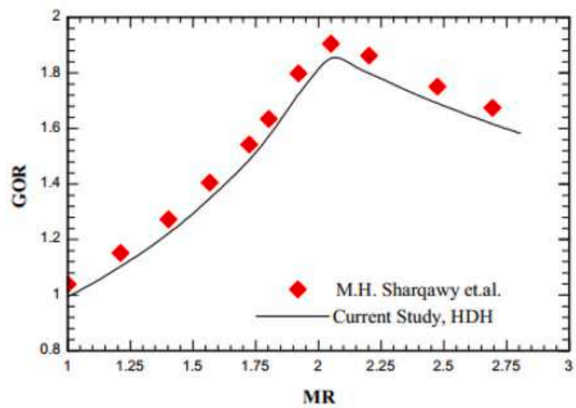

(b) GOR as a function of the MR, based on the present study and compared with results from (Sharqawy et al., 2014).

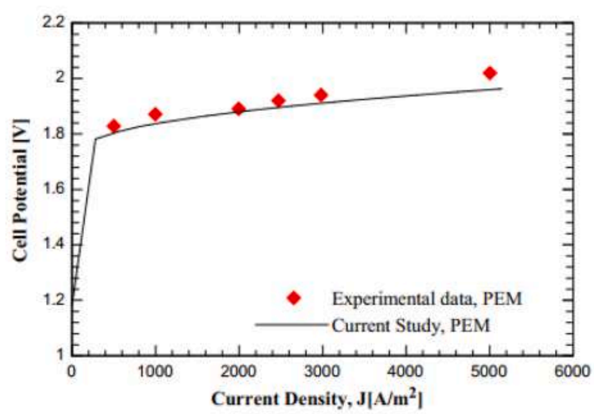

(c) Present study compared with experimental data for the PEM electrolyzer (khanmohammadi and Saadat-Targhi, 2019).

Fig. 4. Validation for each unit in the proposed system.

3.1. Waste heat recovery for electricity generation

The WHR model is exploited to simulate the performance of the WHR system, which utilizes TEG modules arranged in a parallel-flow heat exchanger to recover low-grade waste heat from water vapor mixture heat source as shown in Fig. 2. To make easier the calculation, the next hypotheses are made. Series-connected p-n junctions in the TEG model. Steady-state operation, uniform TEG material properties. Heat losses due to radiation, convection, or conduction between the parallel-flow heat exchanger and its surroundings are assumed to be negligible. Flow behavior at bends within the heat exchanger is simplified, assuming that flow contractions caused by these bends do not impact overall WHR efficiency. The TEG devices are made of numerous pairs of n-type and p-type semiconductor materials arranged in a series configuration.

The TEG model used in this paper (the SP184827145 model) consists of 127 thermocouples based on Bismuth-Telluride (Bi_2Te_3) alloy. These numerous pairs are inserted between electrical conductors and enveloped by insulating layers and ceramic substrates on both hot and cold sides. This structured design facilitates a temperature difference (ΔT)

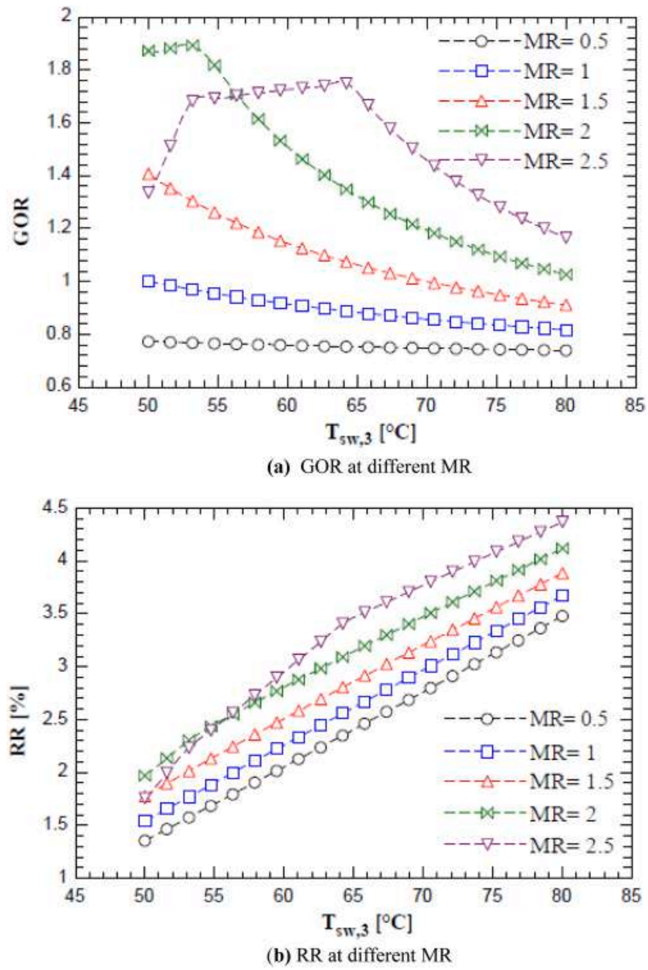

Fig. 5. Performance parameters of the HDH system.

across the TEG surfaces. Table 3 details the **dimensions** of the TEG module.

To explain the heat transfer process within a TEG module, the Eqs. (1) and (2) used to describe the heat is absorbed to hot TEG surface (Q_h), and heat removed from the cold side (Q_c) respectively.

$$Q_h = n\left[\alpha_{pn} \times I \times T_h + K_{pn} \times (T_h - T_c) - 0.5 \times I^2 \times R_{pn}\right] \quad (1)$$

$$Q_c = n\left[\alpha_{pn} \times I \times T_c + K_{pn} \times (T_h - T_c) + 0.5 \times I^2 \times R_{pn}\right] \quad (2)$$

To calculate the different parameters within the TEG module (α_{pn}), (K_{pn}), (R_{pn}) and (I), Eqs. (3) through (6) are used to calculate these factors respectively.

$$\alpha_{pn} = \alpha_p - \alpha_n \quad (3)$$

$$K_{pn} = \frac{(K_p + K_n)A_{leg}}{L_{leg}} \quad (4)$$

$$R_{pn} = \frac{(\rho_p + \rho_n)L_{leg}}{A_{leg}} \quad (5)$$

$$I = \frac{\alpha_{pn}(T_h - T_c)A_{leg}}{L_{leg}} \quad (6)$$

The Seebeck coefficients (α_p, α_n), thermal conductivities (K_p, K_n), and electrical resistivities (ρ_p, ρ_n) for both the (p) and (n) legs are highly dependent on temperature and this variation significantly impacts the performance of the TEG module. Eq. (7) Eqs. (7) through (12) are used for calculating these temperature-dependent properties of the TEG at a

Table 2
Required inputs for thermodynamic modeling.

Parameter	Name	Value	Unit	Reference
Waste heat recovery system				
P_i	Steam inlet pressure	1	atm	
$T_{i,\ hot}$	Steam inlet temperature	100	°C	
m°_{steam}	Steam inlet mass flow rate	20	kg/s	
X_i	Steam quality	0.97	-	
m°_{water}	Cooling fluid mass flow rate	20	kg/s	
$T_{i,\ water}$	Cooling fluid inlet temperature	10	°C	
Humidification dehumidification unit				
$T_{s.\ w,1}$	Seawater inlet temperature	30	°C	
$S_{sw,1}$	Salinity of inlet seawater	35000	ppm	(Sharqawy et al., 2010)
$m^{\circ}_{s.\ w}$	Seawater mass flow rate	0. 0697	kg/s	
ε_h	Humidifier effectiveness	0.85	-	(Prakash Narayan et al., 2010)
ε_d	Dehumidifier effectiveness	0.85	-	(Prakash Narayan et al., 2010)
RH_{a7}	Air relative humidity	100	%	
RH_{a6}	Air relative humidity	100	%	
MR	Mass ratio	2	-	
PEM electrolyzer (khanmohammadi and Saadat-Targhi, 2019; Nami et al., 2017)				
P_{O2}	Oxygen Pressure	1	atm	
P_{H2}	Hydrogen Pressure	1	atm	
L	Membrane thickness	100	µm	
T_{PEM}	Electrolyzer temperature	80	°C	
λa	Water content at the anode interface	14	-	
λc	Water content at the cathode interface	10	-	
$E_{act,\ a}$	Anode activation energy	76	kJ/mol	
$E_{act,\ c}$	Cathode activation energy	18	kJ/mol	
J_a^{ref}	Anode pre-exponential factor	1.764×10^5	A/m^2	
J_c^{ref}	Cathode pre-exponential factor	4.609×10^5	A/m^2	
F	Faraday constant	96485.33	C/mol	
$r_{p-stage}$	Pressure ratio per stage	2.885	-	
R	Universal gas constant	8314.3	J/K. mole	
n	Polytropic index	1.476	-	
η_{comp}	Compressor efficiency	0.95	-	
LHV_{H2}	Lower heating value for hydrogen	120	MJ/kg	
HHV_{H2}	High heating value for hydrogen	142	MJ/kg	

Table 3
Basic parameter TEG module ↱(Khalil and Hassan, 2020).

Parameter	unit	Value
TEG model		SP184827145
PN thermocouples		127 thermocouples
PN dimensions	mm	1.4 × 1.4 × 1.6
Ceramic chip dimensions	mm	40 × 40 × 0.8
TEG dimensions	mm	40 × 40 × 3.9

temperature range of 300 K to 518 K ↱↱(Chen et al., 2011).

$$\alpha_{p(T)} = [5.921376\times10^{-13}\ T^3 - 3.274207\times10^{-9}\ T^2 + 2.422355\times10^{-6}\ T - 2.743842\times10^{-4}] \quad (7)$$

$$\alpha_{n(T)} = [1.291689\times10^{-13}\ T^3 + 1.074408\times10^{-9}T^2 - 9.271759\times10^{-7}T + 8.958888\times10^{-6}] \quad (8)$$

$$\sigma_{p(T)} = [2.248899\times10^{-14}\ T^3 - 1.250867\times10^{-10}\ T^2 + 1.388189\times10^{-7}\ T - 2.244786\times10^{-5}]^{-1} \quad (9)$$

$$\sigma_{n(T)} = [-1.24614\times10^{-14}\ T^3 - 6.429015\times10^{-11}\ T^2 + 9.103036\times10^{-8}\ T - 1.049646\times10^{-5}]^{-1} \quad (10)$$

$$K_{p(T)} = [1.251606\times10^{-7}\ T^3 - 1.242845\times10^{-4}\ T^2 + 3.873788\times10^{-2}\ T - 2.362707] \quad (11)$$

$$K_{n(T)} = [-1.592653\times10^{-8}\ T^3 + 2.905845\times10^{-5}\ T^2 - 1.58323\times10^{-2}\ T + 3.727526] \quad (12)$$

All previously calculated factors can affect the TEG's generated power ($\boldsymbol{P_{net}}$) which depends on the heat transfer process as illustrated in Eqs. (1) and (2). These Equations function in the Seebeck coefficients, thermal conductivities, and electrical resistivities. The Power generated can be calculated by:

$$\boldsymbol{P_{net}} = \boldsymbol{Q_h} - \boldsymbol{Q_c} \quad (13)$$

$$\boldsymbol{P_{elec}} = I^2.\ \boldsymbol{R_{load}} \quad (14)$$

Fig. 3 presents a thermal resistance model for TEG model which the TEG model utilizes aluminum plate-fin heat sinks on both the hot and cold sides of the TEG module, to enhance the TEG system's performance including increasing the net power generated and improving the TEG efficiency. Three different types of thermal resistance can affect the heat transfer processes on both sides: contact thermal resistance (Peterson and Fletcher, 1988) as illustrated in Eq. (15), base material thermal resistance as shown in Eq. (16), and Eq. (17) explain the convection thermal resistance depend on Newton's Law of Cooling (Bergman et al., 2018). In addition to thermal resistance across the TEG hot and cold surface (R_{TEG}) can be calculated from Eq. (18).

$$R_c = \frac{R''_{t,c}}{A_{base}} \quad (15)$$

$$R_b = \frac{L_b}{K_b A_{base}} \quad (16)$$

$$R_{conv} = \frac{1}{h_{conv}\ A_{eff}} \quad (17)$$

$$R_{TEG} = \frac{T_h - T_c}{Q_h - Q_c} \quad (18)$$

$$R_{th,total} = R_c + R_b + R_{conv} \quad (19)$$

Eqs. (20) through (22) are used to calculate the effective heat transfer area (A_{eff}) and fin efficiency (η_f) of the plate-fin heat sinks

$$A_{eff} = (2n\times W_{fin}\times L_{fin})\ \times\eta_f + (n-1)\times W_{fin}\times t_{fin} \quad (20)$$

$$\eta_f = \frac{\tanh m\ \ L_{fin}}{m\ \ L_{fin}} \quad (21)$$

$$m = \sqrt{\frac{2h_{conv}}{K_{fin}.t_{fin}}} \quad (22)$$

Eqs. (23) to (26) provide suitable correlations for calculating the convection heat transfer coefficient in the hot side ($h_{conv,steam}$) ↱↱(Shah, 1979).

$$h_{conv,steam} = h_l\left[1 + \frac{3.8}{Z^{0.95}}\right] \quad (23)$$

$$Z = \left[\frac{1 - X_{inlet}}{X_{inlet}}\right]^{0.8} P_r^{0.4} \quad (24)$$

$$h_l = 0.023\left[\frac{G_m(1 - X_{inlet})D_h}{\mu_l}\right]^{0.8}\left[\frac{\Pr_l^{0.4}\ \ K_l}{D_h}\right] \quad (25)$$

$$G_m = \frac{\mathring{m}_{steam}}{D_h} \quad (26)$$

On the cold side, the Dittus-Boelter equation is a commonly used method for calculating the convection heat transfer coefficient, especially in turbulent flow.

$$Nu = 0.023\ \ \mathrm{Re}^{0.8}\ \ P_r^{0.4} \quad (27)$$

$$h_{conv,cold} = \frac{Nu\times K_{water}}{D_h} \quad (28)$$

The outlet temperature of the cold fluid can be determined by applying Eq. (29). The convective heat transfer coefficient for the hot fluid is expressed in Eq. (30), which depends on the temperature gradient between the hot fluid and the surface temperature of the hot TEG, in addition to the overall thermal resistance. Likewise, the convective heat transfer coefficient for the cold side can be derived using Eq. (31).

$$Q_c = \mathring{m}_{water}\times Cp\times(T_{e,water} - T_{i,water}) \quad (29)$$

$$Q_h = h_{conv,steam} \times A_{teg} \times (T_{steam} - T_h) = (T_{steam} - T_h)/R_{th,total,hot} \quad (30)$$

$$Q_c = h_{conv,cold} \times A_{teg} \times (T_c - T_{water}) = (T_c - T_{water})/R_{th,total,hot} \quad (31)$$

3.2. Humidification- Dehumidification unit

Fig. 1 depicts a water-heated HDH system designed for converting saline water into freshwater. The system comprises a dehumidifier and a humidifier. Saltwater enters the dehumidifier, where it undergoes preheating from the condensing air's latent heat, followed by additional heating using waste heat from the WHR system before being sprayed into the humidifier. In this process, A fraction of the water evaporates into the air, while the left portion is released as brine. Air enters the humidifier, where it undergoes heating and humidification, before being transported to the dehumidifier. In the dehumidifier, water vapor condenses, yielding freshwater. The cycle is sustained by recirculating the cooled air. Several assumptions are applied to model the operation of the HDH unit. The system is assumed to function under steady-state conditions. Heat losses from the components of the HDH unit are considered negligible. Additionally, the energy consumed by seawater pumping and air circulation is assumed to be minimal in comparison to the thermal energy provided to the system (G Prakash Narayan et al., 2010; Prakash Narayan et al., 2013). The temperature of the distillate water at condition 5 is assumed to be the mean value of the dew point of the incoming air and the dry-bulb temperature of the outgoing air (G Prakash Narayan et al., 2010; Prakash Narayan et al., 2010). The salinity of the incoming saltwater to the HDH unit is set at 35 g/kg (Sharqawy et al., 2010). The relative humidity of air exiting both the humidifier and dehumidifier (HRDH) sections is maintained at 100 %. Inlet processes are assumed to occur at constant atmospheric pressure, with feed water and dry air entering the humidifier at near-atmospheric pressures. The HDH model used in this study is a thermodynamic model based on mass and energy balances for each cycle component. To fully analyze the cycle and assess the HDH system's performance, key parameters are required, including the seawater inlet temperature at the dehumidifier, the seawater temperature at the humidifier inlet, and the effectiveness of both the HRDH. The minimum seawater temperature at the dehumidifier inlet varies seasonally, typically between 10°C and 40°C. The maximum seawater temperature at the humidifier inlet is proposed to range from 50°C to 80 °C (Garg et al., 2022). The effectiveness of the HRDH is estimated between 65 % and 95 % (Prakash Narayan et al., 2010). In the HDH system, the dehumidifier (condenser) extracts latent heat from the incoming humid air to produce fresh water. Energy and mass balances, as defined by Eqs. (32) and (33), are used to calculate freshwater production.

$$\mathring{m}_{air}(h_{air,\ 7} - h_{air,\ 6}) = \mathring{m}_{sw}(h_{sw2} - h_{sw1}) + \mathring{m}_{fresh\ water}(h_{fresh\ water,\ 5}) \quad (32)$$

$$\mathring{m}_{fresh\ water} = \mathring{m}_{air}(\omega_{air,\ 7} - \omega_{air,\ 6}) \quad (33)$$

The effectiveness of the dehumidifier component (ε_D) can be defined as (G Prakash Narayan et al., 2010)

$$\varepsilon_D = \max < \frac{(h_{air,\ 7} - h_{air,\ 6})}{(h_{air,\ 7} - h_{air,\ 6ideal})}, \frac{(h_{sw2} - h_{sw1})}{(h_{sw2,ideal} - h_{sw1})} > \quad (34)$$

The outlet air enthalpy at state point 6 is calculated by assuming the air reaches full saturation at the seawater inlet temperature, representing maximum heat transfer from the feed water to the air. Conversely, the ideal seawater outlet enthalpy is calculated by assuming the feed water temperature rises to match the inlet air's dry-bulb temperature at state point 7, indicating maximum heat transfer from the hot air to the seawater. The humidifier in the HDH system transfers heat and moisture to the air by evaporating seawater, which enters at state point 3 and flows over the packing material. Energy and mass balances for the humidifier are calculated using Eqs. (35) and (36).

$$\mathring{m}_{air}(h_{air,\ 7} - h_{air,\ 6}) = \mathring{m}_{sw}(h_{sw3}) - \mathring{m}_{brine,\ 4}(h_{brine,\ 4}) \quad (35)$$

$$\mathring{m}_{brine,\ 4} = \mathring{m}_{sw} - \mathring{m}_{fresh\ water} \quad (36)$$

The humidifier's effectiveness (ε_H) can be expressed as (G Prakash Narayan et al., 2010)

$$\varepsilon_H = \max < \frac{(h_{air,\ 7} - h_{air,\ 6})}{(h_{air,\ 7ideal} - h_{air,\ 6})}, \frac{(h_{sw3} - h_{sw4})}{(h_{sw3} - h_{sw4ideal})} > \quad (37)$$

The heat exchanger raises the seawater temperature from state point 2 (dehumidifier exit) to state point 3 (humidifier inlet at maximum temperature), using water vapor mixture from the WHR system as the heat source. Solving these equations yields several key performance parameters used to assess HDH system performance:

1. Gain-Output Ratio (GOR) relation provides insight into the overall efficiency of the HDH system (G Prakash Narayan et al., 2010; G. Prakash Narayan et al., 2010).
2. Recovery Ratio (RR): The Recovery Ratio (RR) represents the ratio of the produced fresh water to the inlet salt water flow rate within the cycle (A.M.I.Mohamed, 2009).
3. The Mass Flow Rate Ratio (MR) is characterized as the quotient of the flow rate of the incoming saline water to the flow rate of dry air circulating within the HDH cycle (S. Farsad, 2011).

$$GOR = \frac{\mathring{m}_{fresh\ water} . h_{fg}}{Q_{HX,in}} \quad (38)$$

$$RR = \frac{\mathring{m}_{fresh\ water}}{\mathring{m}_{sw}} \quad (39)$$

$$MR = \frac{\mathring{m}_{sw}}{\mathring{m}_{air}} \quad (40)$$

3.3. Hydrogen generation model

The study provides an energy-based analysis to estimate the thermodynamic and electrochemical performance of a PEM electrolyzer system designed for hydrogen generation. The PEM electrolyzer is selected due to its advantages, including its capacity to handle load variations, its compact structure, and its rapid operational response (Nasser et al., 2022a). During the electrolysis process, the PEM electrolyzer requires both electricity and heat to drive the electrochemical reactions. The electricity generated by the WHR system is allocated to power the PEM electrolyzer, pumping process, and the compression or liquefaction of the produced hydrogen. The exhaust steam from the TEGs is used to reheat freshwater generated from HDH unit to the optimal temperature for electrolysis 80°C, which is suitable for operating a PEM electrolyzer at atmospheric pressure. Through the process of electrolysis, water is dissociated into its constituent elements, hydrogen and oxygen. The hydrogen is directed toward the cathode, while the oxygen is channeled to the anode. The initial phase of thermodynamic PEM electrolyzer modeling involves calculating the energy required for hydrogen production (khanmohammadi and Saadat-Targhi, 2019; Nasser and Hassan, 2023). This encompasses both electrical and thermal energy demands, measured in J/mol H2, and can calculated as

$$\Delta H = \Delta G + T\Delta S \quad (41)$$

Where ΔG is the electrical energy request which is equal to the change in Gibbs free energy, and $T\Delta S$ represents the thermal energy required in J/mole H_2.

The hydrogen production rate is determined using current density, Faraday constant, and the rate of H_2O reaction (Ni et al., 2008).

$$\dot{N}_{H_2,out} = \frac{J}{2F} = \dot{N}_{H_2O,reacted} \quad (42)$$

Where J is the current density, F is the Faraday constant, and $\dot{N}_{H_2O,reacted}$ is the rate of H_2O reaction in the process.

Similarly, outlet flow rates of H2O and O2 are computed (Ni et al., 2008)

$$\dot{N}_{O_2,\ out} = \frac{J}{4F} \quad (43)$$

$$\dot{N}_{H_2O,out} = \dot{N}_{H_2O,in} - \frac{J}{2F} \quad (44)$$

Where the flow rate of H_2O at the PEM electrolyzer inlet $\dot{N}_{H_2O,in}$ is a known parameter.

The electrolyzer's electricity (E_{PEM}) requirement is calculated using cell voltage (Razmi et al., 2022).

$$E_{PEM} = J.V \quad (45)$$

The cell voltage(V) comprises reversible potential voltage(V_0), ohmic overpotential(V_{ohm}), and activation overpotential for anode and cathode (V_{act}) (Alirahmi et al., 2020).

$V = V_0 + V_{act,anode} + V_{act,cathode} + V_{ohm}$ (46)The reversible potential voltage is derived from the Nernst equation (Razmi et al., 2022).

$$V_0 = 1.229 - 8.5 \times 10^{-4}(T_{PEM} - 298) \quad (47)$$

Ohmic overpotential comes from membrane resistance to hydrogen ion transport. It depends on humidification degree, membrane thickness (L), and temperature. Local ionic conductivity is expressed as a function of water content (λ(x)) and membrane depth (x) (Gurau et al., 2000).

$$\sigma_{PEM}[\lambda(x)] = [0.5139\lambda(x) - 0.326] * \exp\left[1268\left(\frac{1}{303} - \frac{1}{T_{PEM}}\right)\right] \quad (48)$$

The water content at the cathode and anode interface and membrane thickness can be expressed as (Nasser and Hassan, 2023):

$$\lambda_{(x)} = \frac{\lambda_a - \lambda_c}{L} x + \lambda_c \quad (49)$$

The ohmic resistance can be obtained as follows

$$R_{PEM} = \int_0^L \frac{dx}{\sigma_{PEM}\lambda_{(x)}} \quad (50)$$

The ohmic overvoltage, which results from the resistance of the membrane to the passage of hydrogen ions, is undertaken by Ref. (Nami et al., 2017):

$$V_{ohm} = JR_{PEM} \quad (51)$$

Activation overpotential is calculated using exchange current density (J_0), a crucial parameter indicating electrode capabilities for electrochemical reactions (Ni et al., 2008; Razmi et al., 2022).

$$V_{act,i} = \frac{RT}{F}\sinh^{-1}\left(\frac{J}{2J_{0,i}}\right) i = a, c \quad (52)$$

The exchange current density is expressed using pre-exponential factors (J_i^{ref}) and activation energies (**E_{act}**) for anode and cathode and can be expressed as:

$$J_{0,i} = J_i^{ref}\exp\left(-\frac{E_{act,i}}{RT_{PEM}}\right) i = a, c \quad (53)$$

These calculations collectively form a comprehensive model for PEM electrolyzer performance, integrating various physical and electrochemical parameters to predict system behavior and efficiency.

This module incorporates two primary elements: a compressor and a hydrogen storage tank to retain the generated hydrogen for future utilization. The storage system's compressor derives its energy from the electricity produced by the WHR system, enabling independent operation without grid support. A three-stage multi-stage compressor is employed to compress the produced hydrogen, minimizing energy consumption (Tzimas et al., 2003). Before tank storage, the cooling system reduces the temperature of the hydrogen gas, which possesses a density of 0.0813 g/l at 25 ∘C and 1 bar (Møller et al., 2017). The following equations characterize the compression model (Nasser et al., 2022b; Ozcan and Dincer, 2017; Yavuz, 2020):

$$\dot{W}_{comp} = \frac{\dot{N}_{H_2,out} \times \sum W_{stage}}{\eta_{comp}} \quad (54)$$

$$W_{stage} = \frac{n}{n-1} RT_{in}\left[1 - (r_{p-stage})^{\frac{n-1}{n}}\right] \quad (55)$$

Where W_{stage} represents the work done by each compressor stage (watt), $r_{p-stage}$ denotes the pressure ratio per stage, R is the universal gas constant (J/K.mole), T_{in} signifies the hydrogen temperature (K), n is the polytropic index, η_{comp} indicates the compressor efficiency, and P_{comp} represents the compressor power in (watt).

The storage system can be mathematically represented using either the ideal gas law or the van der Waals equation. Research indicates that both methods yield similar results when the storage pressure is below 200 bar. Following compression, the hydrogen is stored at a pressure not exceeding 200 bar. Thus, the hydrogen storage tank dimensions can be determined using the ideal gas equation as follows (Tzimas et al., 2003)

$$V_{tank} = \frac{\dot{N}_{H_2,out}RT}{P_{tank}} \quad (56)$$

Where $P_{tank}$and V_{tank}represent the hydrogen pressure in the tank (Pa) and volume (m^3), respectively.

3.4. System Performance

The efficiency of the PEM electrolyzer can be calculated (Contreras Bilbao, 2021; G. Basiony et al., 2024)

$$\eta_{PEM} = \frac{HHV_{H2} \times m^{\circ}_{H2,out}}{E_{PEM}} \quad (57)$$

Where HHV_{H2} denotes the higher heating value for hydrogen, and E_{PEM} indicates the electrical energy input to the PEM electrolyzer (kW), and $m^{\circ}_{H2,out}$ is the mass flow rate of hydrogen produced (kg/sec).

To assess the overall efficiency of the integrated Waste Heat Recovery (WHR), Humidification-Dehumidification (HDH), and Proton Exchange Membrane (PEM) electrolyzer system, both energy inputs and useful outputs are evaluated. The primary energy input ($Q_{max,In}$) is taken from the waste heat of saturated steam, calculated as:

$$Q_{max,in} = m^{\circ}_{steam} \cdot (h_{in} - h_{out}) \quad (58)$$

Where m°_{steam} is the steam mass flow rate and h_{inlet} is the specific enthalpy of the steam at the inlet.

The TEGs convert this heat into electrical energy (E_{TEG}), given by:

$$E_{TEG} = \eta_{TEG} \cdot Q_{TEG} \quad (59)$$

Where η_{TEG} is the TEG efficiency, and Q_{TEG} the TEG utilizes thermal energy.

The exhaust steam from the WHR unit is then used to reheat seawater in the HDH process, producing freshwater. The energy associated with this freshwater $E_{freshwater}$is calculated using the latent heat of vaporization:

$$E_{freshwater} = m^{\circ}_{freshwater} \cdot \quad h_{fg} \tag{60}$$

where h_{fg} denotes the latent heat of vaporization (kJ/kg) during the condensation process and its value is extracted directly from EES through its built-in property functions.

To calculate the energy content of the hydrogen produced by the PEM electrolyzer, the mass flow rate of hydrogen ($m^{\circ}_{H2,\ out}$) is used, and the higher heating value (HHV) of hydrogen. The energy content of hydrogen can be calculated as:

$$E\ _{H2} = \quad m^{\circ}_{H2,out}.HHV_{H2} \tag{61}$$

The overall system efficiency ($\eta_{\ overall}$) is then determined by the ratio of the total useful energy outputs (electricity, freshwater, and hydrogen) to the total energy input:

$$E_{useful} = E_{freshwater} + E_{H2} \tag{62}$$

$$\eta_{overall} = \frac{E_{useful}}{Q_{max,in}} = \frac{(m^{\circ}_{freshwater} \cdot\ h_{fg}) + (m^{\circ}_{H2,out}.HHV_{H2})}{(m^{\circ}_{steam} \cdot\ (h_i - h_o))} \tag{63}$$

where h_i is the specific enthalpy of the inlet waste steam to the WHR unit (kJ/kg), h_o is the specific enthalpy of the exhaust steam after all energy recovery stages, including freshwater preheating for PEM operation (kJ/kg).

4. Economic analysis

The economic feasibility of the proposed standalone hydrogen production system is rigorously evaluated using two key economic indicators: Levelized Cost of Hydrogen (LCOH) and Net Present Value (NPV). These metrics assess the system's cost efficiency and long-term financial sustainability, considering capital investments, operational expenses, and the time value of money.

The proposed system integrates a waste heat recovery (WHR) unit that utilizes thermoelectric generators (TEGs) to convert waste heat into electricity, which is then used to power a proton exchange membrane (PEM) electrolyzer for hydrogen production. A humidification-dehumidification (HDH) unit supplies the required freshwater for electrolysis, ensuring the system's self-sufficiency without reliance on external power or water sources. The Levelized Cost of Hydrogen (LCOH) represents the average cost of hydrogen production over the system's operational lifespan, normalized per kilogram of hydrogen. This metric accounts for initial capital expenditures, operational and maintenance (O&M) costs, and energy efficiency, comprehensively evaluating the system's economic competitiveness against conventional hydrogen production methods(Rezaei et al., 2020).

$$LCOH\left(\frac{\$}{kg}\right) = \frac{I + \sum_{n=1}^{N} \frac{I_{o\&M}}{(1+r)^n}}{\sum_{n=1}^{N} \frac{H_{2,annual}}{(1+r)^n}} \tag{64}$$

Where I, is the project capital cost, $I_{o\&M}$ is the operation and maintenance cost and $H_{2,annual}$ is the annual hydrogen production.

Meanwhile, the Net Present Value (NPV) analysis quantifies the system's profitability, determining the break-even period and long-term financial viability under varying hydrogen price scenarios. By leveraging waste heat to generate electricity and freshwater for electrolysis, the proposed system offers a cost-effective and energy-efficient alternative for hydrogen production. Its economic and environmental advantages position it as a sustainable solution for integrating renewable hydrogen into industrial and energy sectors. The NPV at year n may be calculated as follows (Dehwah et al., 2020; Manzotti et al., 2022):

$$NPV(\$) = -I + \sum_{n=1}^{N} \frac{B(n)}{(1+r)^n} \tag{65}$$

The net cash flow of a specific year is expressed by B(n).

Key parameters for the economic evaluation are provided in Tables 4 and 5.

Table 4
Economic parameters.

Parameter	Value	Ref
Annual operating hours	**8000 h**	(Mohammadi and Mehrpooya, 2019)
Discount rate (r)	**10 %**	(Egypt., 2025)
Project lifespan (N)	**20**	(Mohammadi and Mehrpooya, 2019)

Table 5
Capital cost breakdown.

Unit	Component	Initial Cost $	O&M cost	Reference
WHR	**TEG**	0.68$	0 %	(Ahmed et al., 2023; "Thermoelectric Peltier Power Generator Sp1848–27145 Superconducting Heat Series - Buy Sp1848–27145,Sp1848 27145,Peltier Sp1848–27145 Product on Alibaba.com," n.d.)
	Heat Sink	0.77$		(Ahmed et al., 2023; "Custom High Power 40x40mm Heat Sink Extrusion Aluminium Led Heatsinks Pcb Heatsink Aluminum - Buy Heatsink Aluminum 40x40mm heatsink For Laptop led Heatsinks Pcb Product on Alibaba.com," n.d.)
	Heat Exchanger	$200A_{HX,WHR}$	1 %	(ENERGY, 2025)
	Pump	150$	1 %	(B. Kariuki et al., 2024)
HDH	**Humidifier**	133$	10 %	(Kahani et al., 2024; B. Kariuki et al., 2024)
	Dehumidifier	500$		(B. Kariuki et al., 2024)
	Heat Exchanger	$350A_{HX,HDH}$		(ENERGY, 2025)
	Pumps and blowers	345$		(Abu El-Maaty et al., 2024; B. Kariuki et al., 2024)
	Water Tank	260$		(Abu El-Maaty et al., 2024; B. Kariuki et al., 2024)
	Others (Labor, piping, etc.)	550$		(B. Kariuki et al., 2024)
PEM	**PEM Electrolyzer**	1000 $/kW	6 %	(G. Basiony et al., 2024)(Nasser and Hassan, 2023)
	Heat exchanger	$350A_{HX,HDH}$		(ENERGY, 2025)
	Pump	150$		(B. Kariuki et al., 2024)
	Hydrogen storage Tank	500$/kg		(G. Basiony et al., 2024)

5. System solution and validation

A comprehensive numerical model was developed and implemented in MATLAB to simulate the integrated WHR, PEM electrolyzer, and HDH systems. The model leverages the XSteam package® (Holmgren, 2024) to calculate water and steam properties based on the IAPWS IF-97 standard, ensuring accurate thermodynamic evaluation.

The WHR system, consisting of TEG modules arranged in four configurations, is modeled using iterative methods programmed and solved in MATLAB. The solution simultaneously satisfies energy balance equations on both the hot and cold sides of each TEG module and accounts for heat dissipation into the external electrical load. The model calculates the electric current, hot and cold side temperatures, and overall TEG power output. Validation of the WHR model was carried out by comparing results against experimental data from (Khalil and Hassan, 2019), with strong agreement observed, as shown in Fig. 4a.

For the HDH desalination unit, the Engineering Equation Solver

(EES) software was used to solve the governing thermodynamic equations through an iterative convergence scheme. EES uses robust correlations for seawater and moist air properties from Sharqawy et al. (2010) and Hyland and Wexler (1983), respectively. The HDH model is validated against a simplified thermodynamic model from (Sharqawy et al., 2014), with results shown in Fig. 4b demonstrating high accuracy.

The PEM electrolyzer subsystem was developed and solved in MATLAB. The validation of the PEM model was conducted by comparing simulation results of current density and cell potential with experimental data (khanmohammadi and Saadat-Targhi, 2019). The results from the simulations depicted in Fig. 4c are in close agreement with the experimental data, showing a maximum deviation of less than 3 %. This indicates that the predictions regarding the performance of the electrolyzer are reliable. Fig. 4c illustrates the characteristic polarization curve, which depicts the relationship between current density (J, A/m^2) and cell voltage (V) for the PEM electrolyzer. As current density increases, cell voltage also rises. This behavior is consistent with both electrochemical theory and experimental findings. The increase in voltage can primarily be attributed to a combination of activation overpotentials, ohmic losses, and concentration polarization that occurs at higher current densities. At lower current densities, the rise in cell voltage is gradual, indicating low activation losses. However, as current density increases, the voltage rise becomes more pronounced due to greater resistive (ohmic) and mass transport challenges. This pattern confirms that the developed model accurately reflects the nonlinear characteristics of the PEM cell, encompassing both kinetic and transport-related losses. The strong correlation between the simulated and experimental results across the entire range of current densities validates the model, making it suitable for predicting the electrolyzer's performance under various operating conditions within the overall system.The strong agreement between simulated and experimental data for all three subsystems (TEG, HDH, and PEM) ensures the credibility of the integrated system model used in this study.

6. Results and discussions

The system under consideration integrates three primary components: a Waste Heat Recovery (WHR) mechanism, an HDH process, and a hydrogen production unit. The principal parameters examined include the steam mass flow rate, which is adjusted between 5 and 20 kg/sec, and the steam inlet quality ranges from 0.05 to 0.97. The steam inlet temperature is maintained at a constant 100°C. In contrast, the cooling fluid temperature remains steady to isolate the effects of steam mass flow rate and inlet quality on system performance. The objective is to determine the configuration that yields maximum power generation from the WHR system.

Following identifying the optimal power generation configuration, the research evaluates the effects of varying the steam inlet temperature from 100°C to 160°C while considering different steam inlet quality values (0.05–0.97). This analysis will elucidate the influence of temperature changes on power generation, overall hydrogen production, and system efficiency. The thermal energy exhausted from the WHR system will be used to reheat the maximum brine temperature before entering the HDH unit's humidifier for freshwater production. The resulting freshwater will subsequently generate hydrogen through a Proton Exchange Membrane (PEM) electrolyzer. The freshwater will be heated to the PEM's operating temperature of 353 K using thermal energy exhaust from the WHR system to reheat the brine before entering the PEM.

6.1. HDH desalination

6.1.1. CAOW performance analysis

This study focuses on the performance analysis of a Closed-Air Open-Water (CAOW) water-heated system within the HDH process. The study assesses GOR across several operational parameters, including the ratio of saline water mass flow rate to dry airflow, top brine temperature, and seawater inlet temperature. To examine the impact of varying mass flow rate ratios on the HDH system's performance, GOR, and RR are analyzed under baseline conditions, which include a seawater inlet (bottom) temperature of $T_{sw,1}$= 30°C, a seawater mass flow rate of 0.0697 kg/s, and humidifier and dehumidifier effectiveness set at 0.85. Performance is also evaluated at different seawater inlet temperatures to the humidifier. The performance figures presented in this study, such as Figs. 5a and 5b, are descriptive and offer key insights into the underlying thermodynamic behavior of the HDH system. A detailed analysis of these figures highlights critical design and operational implications.

Fig. 5a demonstrates the relationship between the mass flow rate ratio (MR), top brine temperature ($T_{sw,3}$), and the Gained Output Ratio (GOR) of the HDH system. For MR >1, GOR initially rises with increasing $T_{sw,3}$, peaking at an optimal temperature before declining. This trend arises from a thermodynamic balance between heat input and distillate enthalpy. At lower temperatures, distillate enthalpy increases faster than heat input, improving GOR. Beyond the optimal $T_{sw,3}$ (dependent on MR), heat input outpaces enthalpy gains, reducing GOR due to disproportionate thermal energy demands. For example, at MR = 2.5, elevating $T_{sw,3}$ enhances evaporation and GOR, while lower MR values (e.g., 0.5, 1) shift the optimal $T_{sw,3}$ downward, as higher dry air flow improves heat/mass transfer efficiency at reduced brine temperatures.

The interplay between MR and thermal efficiency further governs system performance. Higher MR shortens brine residence time in the humidifier, limiting vaporization efficiency, whereas lower MR (or increased dry air flow) extends heat exchange duration, improving evaporation even at lower $T_{sw,3.}$ This explains the inverse correlation between optimal $T_{sw,3,}$ and MR.

Fig. 5b illustrates the recovery ratio (RR) as a function of $T_{sw,3}$. RR consistently increases with temperature, driven by intensified evaporation (via Clausius-Clapeyron-driven vapor pressure rise) and condensation efficiency. However, at MR = 2.5, RR declines between 50 °C and 54.74 °C due to energy demands outstripping distillate gains, highlighting a trade-off between throughput and efficiency. While elevated $T_{sw,3}$ maximizes RR, it often reduces GOR, necessitating operational prioritization: higher temperatures favor distillate quantity (RR), while moderate temperatures favor energy efficiency (GOR). The system achieves peak GOR (1.892) at $T_{sw,3}$= 53.16°C and MR = 1.892, with a brine exit temperature of 37.2°C. This equilibrium ensures sufficient humidification without energy waste, avoiding dry air (low MR) or excessive heating (high MR). These findings underscore the necessity of optimizing MR and $T_{sw,3}$ to align with desalination objectives—maximizing yield or efficiency—based on resource constraints.

This performance metric highlights a critical trade-off between the Gain Output Ratio (GOR) and Recovery Ratio (RR). While the RR generally improves with elevated top brine temperatures, the GOR serves as an indicator of the thermal efficiency of the Humidification-Dehumidification (HDH) process and becomes a more decisive metric when system performance is constrained by limited thermal input, such as waste heat. A higher GOR signifies that more freshwater is produced per unit of heat input, which is crucial for maximizing the utility of low-grade thermal energy. Consequently, selecting the operating point that maximizes the GOR ensures a balance between adequate freshwater generation and optimal utilization of available thermal energy—both essential for subsequent stages involving hydrogen production and power generation.

6.1.2. Sensitivity of CAOW HDH cycle to seasonal and climatic variability

The efficiency of HDH desalination systems, especially the CAOW setup, is significantly impacted by changes in seasons and climate, as shown in Fig. 6. Fluctuations in ambient temperature and relative humidity (RH) have a direct impact on the Gained Output Ratio (GOR), a vital indicator of system performance. For instance, Fig. 6a demonstrates that raising the saline water inlet temperature ($T_{sw,1}$) from 25°C

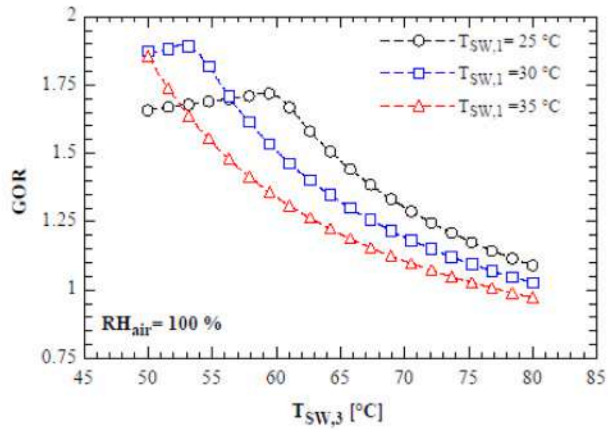

(a) Impact of saline water inlet temperature ($T_{sw,1}$) on optimal humidifier inlet temperature ($T_{sw,3}$) and GOR at RH = 100%.

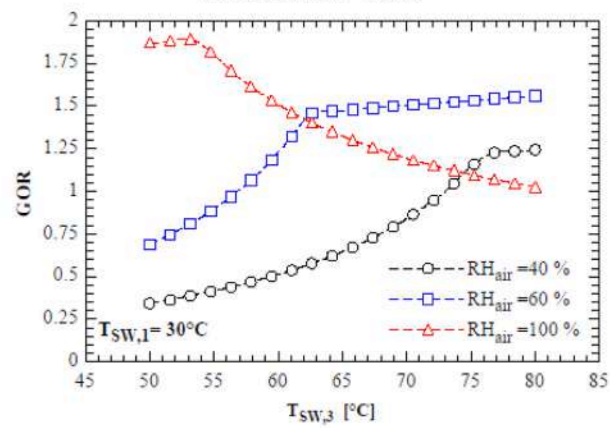

(b) Impact of change relative humidity on GOR with humidifier inlet temperature ($T_{sw,3}$) at $T_{sw,1}$ = 30 °C

Fig. 6. Influence of seasonal and climatic variability on the performance of the CAOW HDH desalination system.

to 35°C while maintaining a constant RH of 100 % changes the optimal humidifier inlet temperature ($T_{sw,3}$) needed to achieve the highest GOR. When $T_{sw,1}$ is 30°C, the system reaches a maximum GOR of 1.892 with $T_{sw,3}$ set at 53.16°C, reflecting an ideal balance between thermal energy input and freshwater output. However, further increases in $T_{sw,1}$ lead to decreased efficiency due to thermal saturation and increased irreversibilities, in line with the Second Law of Thermodynamics. Relative humidity is also crucial to system performance. Under saturated conditions (RH = 100 %), the air's ability to absorb more vapor is limited, even at higher temperatures, causing a drop in GOR beyond the optimal point. In contrast, at lower RH levels (40 % or 60 %), as depicted in Fig. 6b, drier air allows for more moisture absorption, promoting better evaporation and higher GOR values at increased $T_{sw,3}$. This effect is especially notable in dry climates, where the GOR at RH = 40 % and $T_{sw,3}$ = 80°C can surpass that under saturated conditions. While this performance boost aligns with the Clausius-Clapeyron relation—showing that vapor pressure rises exponentially with temperature—it also leads to greater energy use. These results highlight the necessity of climate-adaptive operation for HDH systems. In humid areas, moderate temperatures around 50–55°C are adequate for optimal performance, whereas arid regions require higher operating temperatures to sustain productivity. The use of waste heat in these climates can help mitigate the additional energy requirements. Ultimately, incorporating climate-responsive control strategies is crucial to ensure consistent and efficient system performance across diverse environmental conditions.

6.2. Waste heat recovery performance

6.2.1. WHR configuration performance

The study conducted a detailed analysis of four distinct system configurations, as shown previously, to evaluate their power generation capabilities. Each configuration is initially assessed when a steam mass flow rate changes from 5 to 20 kg/s at a cooling water flow rate of 20 kg/s.

Figs. 7a–7d illustrate how steam inlet quality and mass flow rate influence net power output across the four WHR configurations. A general trend observed in all cases is that increasing both parameters leads to higher power generation due to enhanced latent heat availability for thermoelectric conversion. Higher steam dryness fractions contain more latent heat, improving heat transfer to the TEG's hot surface, as described in Eq. (23). Second, the rise in the convection heat transfer coefficient with increasing steam quality reduces the thermal resistance on the hot side, resulting in improved heat transfer and power generation, as indicated by Eq. (13). The arrangement of TEG modules within the heat exchanger significantly affects the system's ability to extract latent heat from the steam, which impacts the net power output. Configurations with greater TEGs in the longitudinal direction (aligned with the steam flow) and fewer in the lateral direction improve power generation. For instance, Configuration-1, with an equal number of TEGs in both directions (100 ×100), produces less power due to the uniform steam flow distribution. In contrast, Configuration-4 (12 ×833) shown in Fig. 7d, achieves higher power output due to more effective latent heat extraction, facilitated by the varying enthalpy distribution

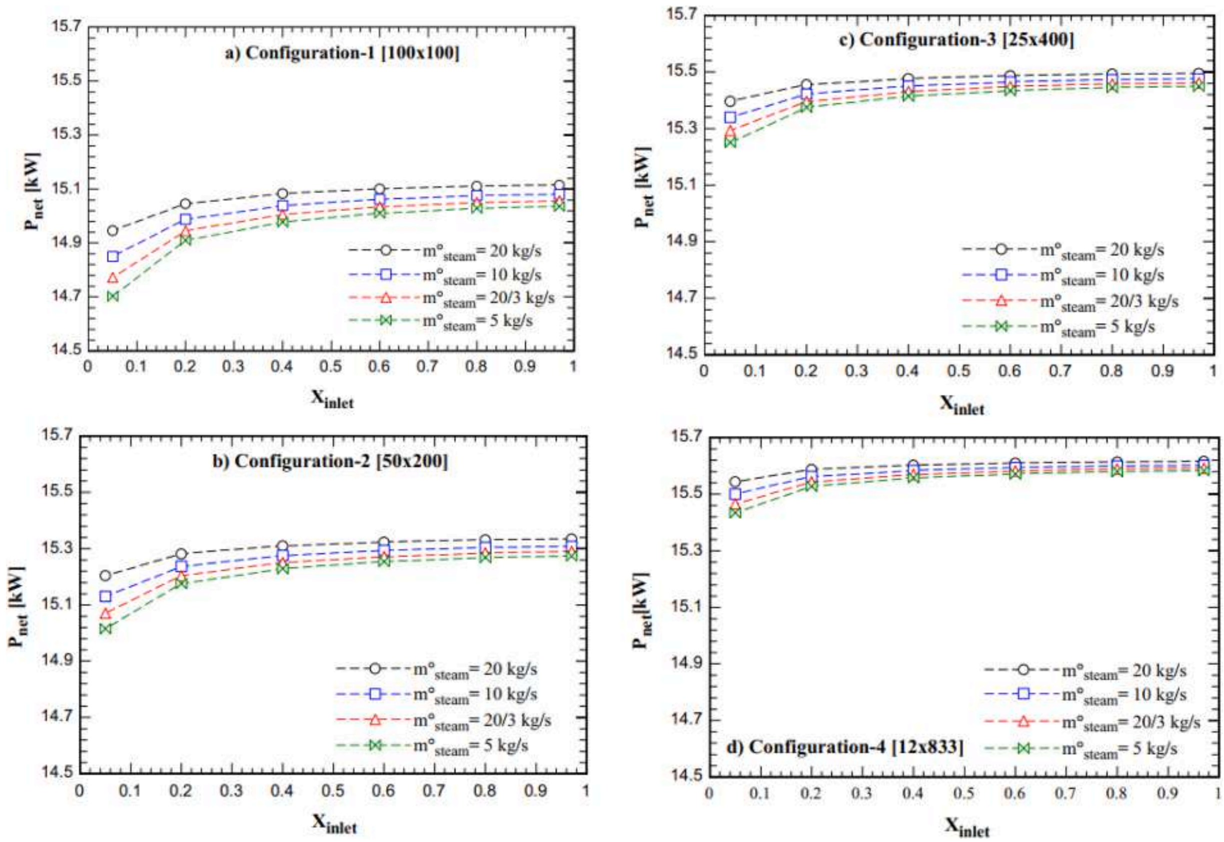

Fig. 7. Impact of steam inlet quality on net power generation for different configurations.

across the TEG modules. A key example of this is the increase in net power output from 15.11 kW to 15.62 kW when shifting from Configuration-1 (100 ×100) to Configuration-4 (12 ×833) at a steam inlet quality of 0.97 and a steam flow rate of 20 kg/s.

Configuration-4 extracts more energy from the steam (337 kW) than Configuration-1. (332 kW), contributing to the observed increase in power output. This trend is also evident at lower steam qualities; for instance, at a steam inlet quality of 0.05 and a steam flow rate of 20 kg/s, net power output increases from 14.95 kW in Configuration-1–15.54 kW in Configuration-4. Increasing the steam flow rate further enhances power generation, as a greater mass flow results in more latent heat transfer through the TEG modules. In Configuration-2 (Fig. 7b), for example, increasing the steam flow rate from 5 kg/s to 20 kg/s at a steam inlet quality of 0.97 results in a net power increase from 15.27 kW to 15.4 kW, demonstrating improved heat utilization.

Configuration-4 consistently demonstrates the highest power generation at different steam flow rates among all the configurations. At a steam inlet quality of 0.97 and a steam flow rate of 20 kg/s, Configuration-4 produces 0.5 kW more power than Configuration-1, 0.27 kW more than Configuration-2, and 0.121 kW more than Configuration-3. This superior performance is primarily attributed to the longitudinal arrangement of the TEG modules, which enables more efficient latent heat extraction and better steam flow distribution. Therefore, Configuration-4 is the most effective configuration for maximizing power generation under various operational conditions, particularly at different steam mass flow rates.

6.2.2. Thermal sensitivity of the WHR-TEG system

Following a comprehensive comparison, Configuration 4 emerged as the most effective in maximizing power output, making it the preferred choice for further investigation. In the next phase of the study, the analysis focuses on how variations in steam inlet temperature (100°C to 160°C), steam inlet quality (0.05–0.97), and steam mass flow rate (2–20 kg/s) influence power generation in the selected configuration. Although heat losses to the environment were neglected in the WHR model to focus on ideal system performance, temperature-dependent thermoelectric material properties were retained to ensure a realistic representation of TEG behavior. Specifically, the Seebeck coefficient, thermal conductivity, and electrical resistivity were calculated as functions of the temperature between the hot and cold surfaces of the TEG based on established polynomial correlations ↱↱(Chen et al., 2011). This approach enables the model to reflect the non-linear behavior of thermoelectric modules across a wide range of thermal operating conditions.

Fig. 8 provides critical insights into these dynamics, illustrating the interplay between steam inlet parameters and system performance. Among the key findings, steam inlet temperature exhibits the most dominant influence on power generation. As the temperature gradient across the TEG increases—driven by the Seebeck effect—the net power output rises significantly. For instance, Fig. 8e shows that at a steam flow rate of 20 kg/s and inlet quality of 0.97, increasing the steam temperature from 100°C to 160°C boosts the power output from 15.615 kW to 36.881 kW, marking a 130 % increase. At lower steam qualities, condensation dynamics introduce additional complexity. Fig. 8a highlights that at a flow rate of 2 kg/s and steam quality of 0.05, increasing the inlet temperature leads to a slight reduction in power generation. This is attributed to the shift from latent heat transfer—characterized by a higher heat transfer coefficient—to sensible heat transfer once the steam fully condenses at saturation. The position of the condensation front along the TEG array, as shown in Table 6, significantly affects the thermal gradient and, thus, the power output. For instance, at 160 °C and 5 kg/s, condensation occurs after approximately 744 TEG modules, leaving the remaining modules to operate under lower-efficiency sensible heat transfer. On the other hand, increasing steam inlet quality at a constant temperature (100°C) enhances power generation due to higher latent heat content. Fig. 7b demonstrates that raising quality from 0.05 to 0.97 at 5 kg/s results in an output increase from 15.43 to 15.583 kW.

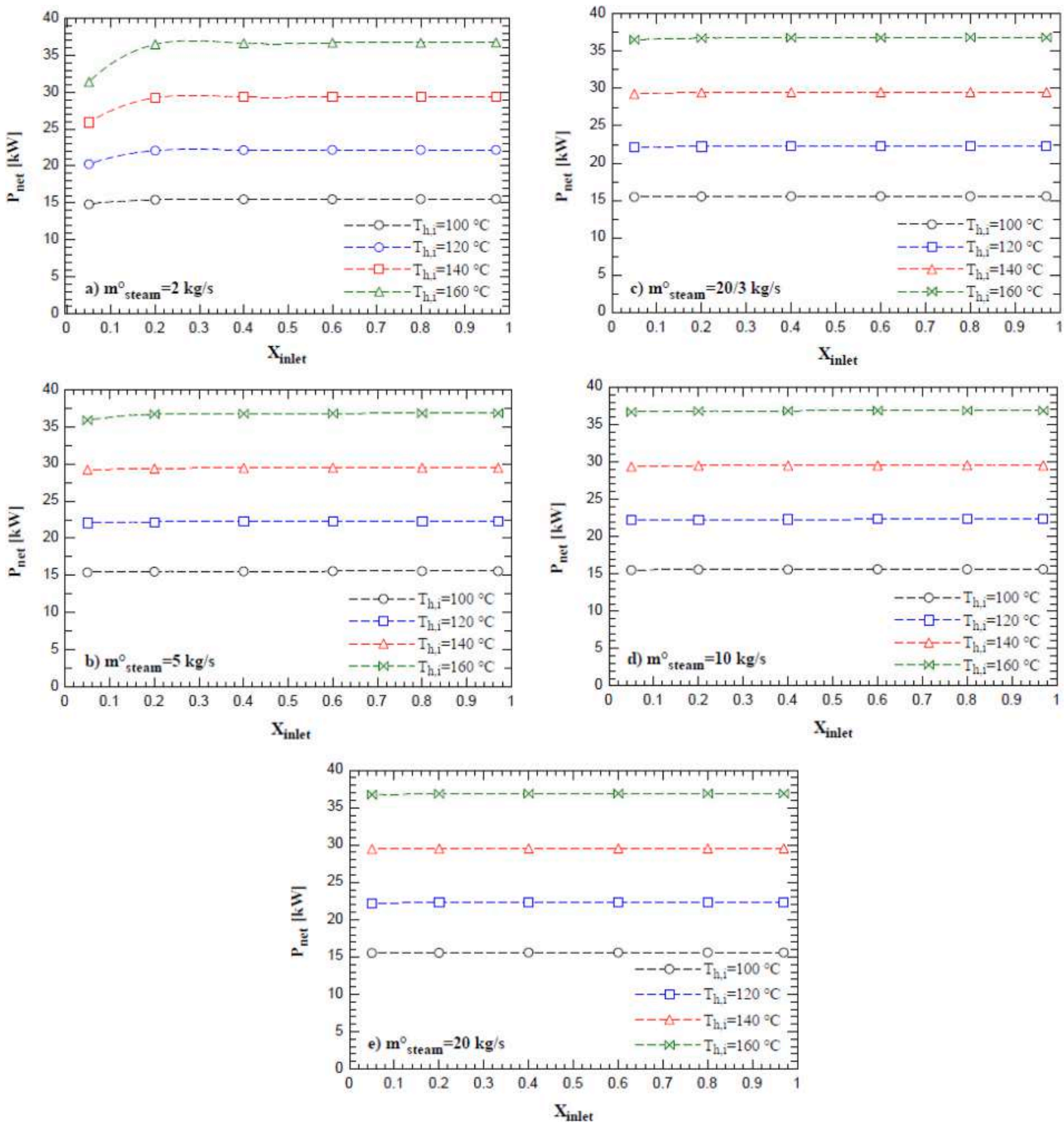

Fig. 8. Impact of steam inlet temperature on the net power generated for the best configuration.

Table 6
Impact of steam inlet temperature on steam condensation properties.

$T_{h,\ i}$ [°C]	m°_{steam} [kg/sec]	X_{inlet}	TEG $_{latent\ heat}$	TEG $_{sensible\ heat}$	$T_{h,\ exit}$ [°C]
100	2	0.05	559	274	87.82
120	2		444	389	99.857
140	2		360	473	111.76
160	2		295	538	123.48
	5		744	89	144.1014

Similarly, increasing the mass flow rate from 5 to 20 kg/s at the fixed quality (0.97) and temperature (100°C) marginally improves output from 15.583 to 15.62 kW (Fig. 8e) due to the higher rate of thermal energy delivery.

Overall, the results confirm a consistent trend: power generation improves significantly with increasing steam inlet temperature and, to a lesser extent, with higher quality and mass flow rate. Using temperature-dependent thermoelectric properties ensures the model's sensitivity to these variations while idealizing heat losses provides an upper-bound system performance estimation. These findings reinforce the suitability of Configuration 4 and provide a strong basis for optimizing WHR-TEG integration under diverse thermal input scenarios.

6.3. Hydrogen production system

6.3.1. Performance analysis of hydrogen production

Following the production of purified water via the HDH unit and electricity generation from the WHR system, the final stage of the process involves hydrogen production using a PEM electrolyzer. The integration of outputs from both the HDH and WHR systems plays a critical role in achieving the overarching goal of sustainable hydrogen production. Specifically, the PEM electrolyzer utilizes purified water from

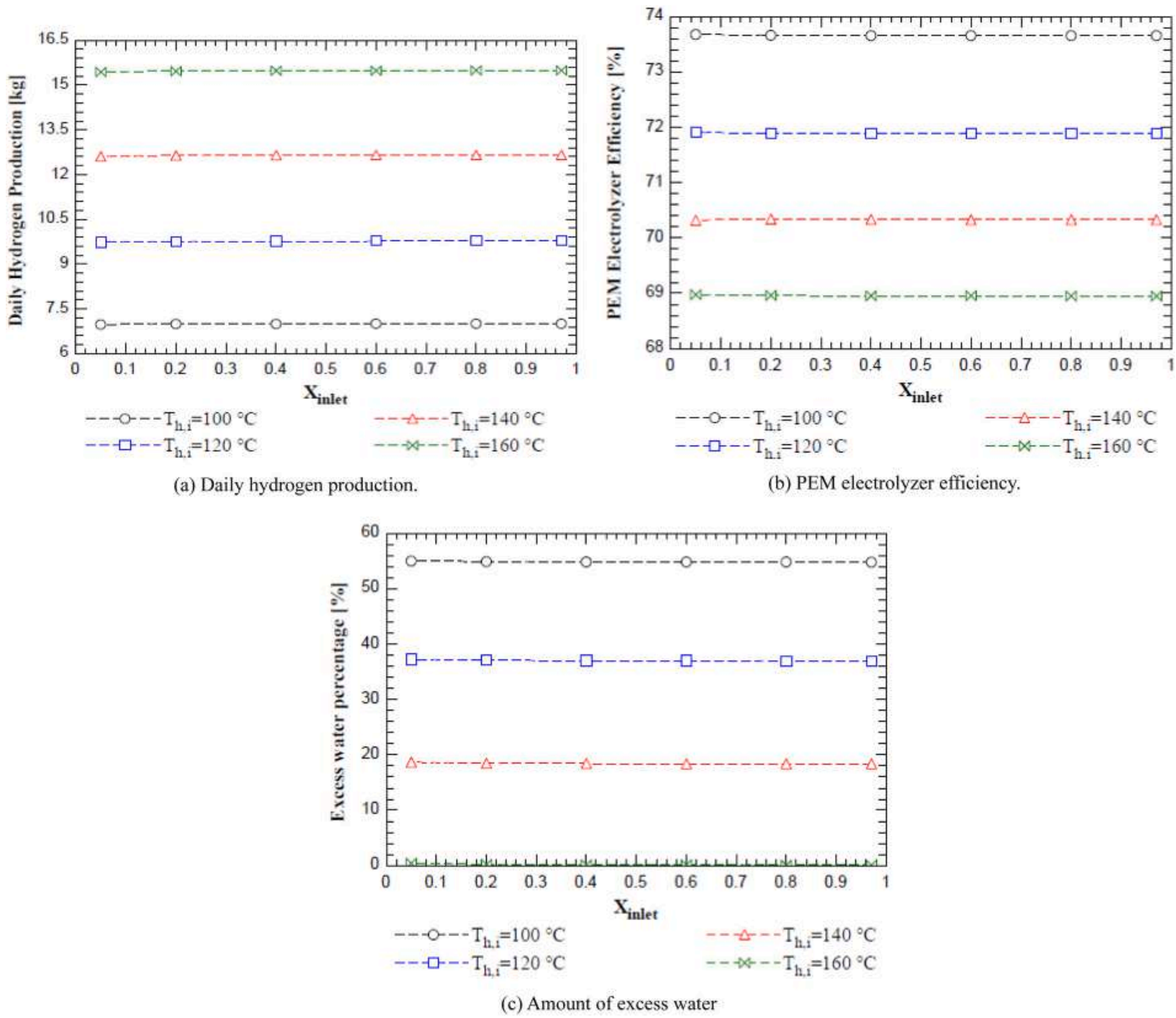

Fig. 9. Impact of steam inlet temperature on the hydrogen production unit parameters.

the HDH unit as feedstock for the electrolysis process. At the same time, the electricity generated by the WHR system powers the electrolyzer, enabling the efficient splitting of water molecules into hydrogen and oxygen. This integrated approach maximizes resource utilization and underscores the potential for creating a closed-loop system that minimizes external energy inputs and reduces environmental impact. The overall efficiency of the system is highly dependent on the careful management of water and energy inputs to meet the operational demands of the electrolyzer, particularly under varying parameters such as steam inlet temperature (ranging from 100°C to 160°C) and steam inlet quality (ranging from 0.05 to 0.97) at a steam mass flow rate of 20 kg/s.

Figs. 9a through 9c illustrate the relationship between steam inlet quality, temperature, daily hydrogen production, PEM electrolyzer efficiency, and the percentage of excess water at a fixed steam mass flow rate of 20 kg/s. The results indicate that increasing steam inlet temperature enhances daily hydrogen production, as shown in Fig. 9a, a trend largely driven by thermodynamic efficiency. According to the Second Law of Thermodynamics, a larger temperature differential across the TEG increases its ability to convert thermal energy into electrical power. As the steam inlet temperature rises, the higher energy input generates more electricity, boosting the hydrogen production rate. The influence of steam quality also plays a crucial role in energy availability. Steam quality directly affects the amount of latent heat available for recovery in the WHR system. At higher steam qualities, more latent heat is available for conversion into electrical energy, as the water vapor mixture carries more energy in latent heat than with lower quality, where liquid droplets reduce energy efficiency. For instance, at a steam inlet temperature of 100°C, increasing the steam inlet quality from 0.05 to 0.97 results in a rise in hydrogen production from 6.9744 kg/day to 7.0056 kg/day, as shown in Fig. 9a. This improvement is associated with an increase in the power output of the TEG, from 15.543 kW to 15.615 kW, due to the higher recoverable energy in higher-quality steam. The relationship between temperature and hydrogen production becomes more pronounced at higher temperatures. At 160°C, the temperature differential across the TEG significantly enhances power generation. For example, at a steam inlet quality of 0.97 and a mass flow rate of 20 kg/s, the net power output increases from 15.615 kW at 100°C to 36.881 kW at 160°C, representing a more than 130 % increase. This sharp rise in power output leads to a corresponding increase in daily hydrogen production, from 7.0056 kg/day to 15.4872 kg/day, as illustrated in Fig. 9a. This illustrates how the system's performance is strongly influenced by both temperature and quality parameters, with temperature having a dominant effect due to its role in optimizing thermoelectric power generation. The modest increase in hydrogen production at lower temperatures and varying steam qualities highlights the system's sensitivity to operational conditions. At lower temperatures, the available energy for conversion is diminished, making the system more responsive to steam quality changes. As the temperature increases, however, the influence of steam quality becomes less significant relative to the temperature-driven thermoelectric effect. From an electrochemical standpoint, the power supplied to the PEM electrolyzer is a key determinant of hydrogen production.

According to Faraday's Law of Electrolysis, the hydrogen generation rate is proportional to the amount of electric charge passed through the electrolyzer. As the power generated by the WHR system increases, the current supplied to the PEM electrolyzer also increases, driving higher hydrogen production rates.

Fig. 9b illustrates the efficiency of the PEM electrolyzer is significantly influenced by the power supplied from the WHR system, which is determined by both the steam inlet temperature and steam quality. The general trend observed is that while increasing steam inlet temperature significantly enhances power generation and hydrogen production, it leads to a corresponding decline in PEM electrolyzer efficiency due to higher overpotentials, thermal degradation, and ohmic losses. Conversely, lower steam qualities at fixed temperatures result in a slight improvement in efficiency, highlighting the importance of balancing power input and system stability for optimal performance.

At a steam inlet temperature of 100°C and steam quality of 0.97, the PEM electrolyzer achieves an efficiency of 73.653 %. As the steam inlet quality decreases to 0.05 at the same temperature, the efficiency slightly increases to 73.6743 %. This small rise in efficiency is due to the power reduction generated by the WHR system, where the power output decreases from 15.615 kW to 15.543 kW. The reduced power input to the PEM electrolyzer leads to a more stable electrolysis process, slightly improving the overall efficiency.

A more pronounced change in PEM electrolyzer efficiency occurs as the steam inlet temperature increases. At 160°C and steam inlet quality of 0.97, the efficiency drops to 68.94 %, despite the significant rise in power generation, which reaches 36.881 kW. This decline has several causes. First, at higher power inputs, particularly at elevated temperatures, the overpotentials at the anode and cathode of the PEM electrolyzer increase. These overpotentials, linked to reaction kinetics and mass transport limitations, cause energy losses that reduce the system's efficiency. The electrolysis process becomes less efficient as the current density rises with higher power input, contributing to the observed efficiency drop. The increased operating temperature (160°C) also affects the proton exchange membrane and the catalyst layers within the PEM electrolyzer. Higher temperatures can accelerate membrane degradation and reduce catalyst performance, leading to lower proton conductivity and decreased reaction efficiency. This thermal degradation explains the efficiency drop at higher temperatures, as the electrolyzer operates outside its optimal thermal range.

In addition, as power input increases, the current density supplied to the PEM electrolyzer rises, resulting in greater ohmic losses within the system. These losses, stemming from the resistance to the flow of protons through the membrane and electrons through the external circuit, become more significant at higher current densities. The increased internal resistance directly reduces the electrolyzer's efficiency, particularly when operating at elevated power levels.

Finally, decreased PEM efficiency at higher steam temperatures and power inputs indicates the classic trade-off between power density and efficiency in electrochemical systems. As the system generates more power, the losses (due to ohmic resistance, overpotentials, and heat) increase disproportionately, resulting in lower efficiency despite higher hydrogen production rates.

The modest increase in efficiency at lower steam qualities, particularly at 100°C, suggests that optimizing steam quality can improve PEM electrolyzer performance under specific conditions. Lower steam qualities lead to reduced power generation, stabilizing electrolysis and mitigating some efficiency losses observed at higher temperatures. This emphasizes the importance of managing steam inlet parameters to balance power generation and electrolyzer efficiency.

Fig. 9c illustrates the variation in excess water percentage exiting the PEM electrolyzer at different steam inlet temperatures and qualities. A general trend shows that the excess water percentage slightly increases as the steam inlet quality decreases. This is due to reduced power generation at lower steam qualities, leading to less water consumption in the electrolysis process. However, the most notable trend is the significant decrease in excess water percentage with increasing steam temperature. The percentage of excess water decreases with increasing steam inlet temperature. At higher power outputs, the PEM electrolyzer generates more hydrogen, which requires more water for the electrolysis process at the cathode and anode. As hydrogen production increases, more water is consumed, leaving less excess water in the system. At higher steam temperatures, the increased power output drives a greater hydrogen production rate, demanding more water for the water-splitting reaction ($2H_2O \rightarrow 2H_2 + O_2$). Higher hydrogen generation results in more water consumption, reducing excess water percentage. Less hydrogen is produced at lower temperatures and power outputs, and more water remains unconsumed, contributing to the observed excess water. Additionally, the PEM electrolyzer operates more efficiently due to improved proton conductivity and enhanced catalyst activity. For example, at a steam inlet temperature of 160°C, the excess water percentage approaches nearly zero, indicating that the PEM electrolyzer utilizes almost all the inlet water for hydrogen production. In contrast, at a lower steam temperature of 100°C, the excess water percentage reaches approximately 55 % when the steam inlet quality is 0.05. The slight increase in excess water percentage at lower steam qualities is directly tied to the lower power generation by the WHR system. As power generation decreases, the PEM electrolyzer operates at a lower current density, producing less hydrogen and consuming less water, leaving more excess water in the system.

6.3.2. *Hydrogen storage challenges*

The interaction between steam parameters and the efficiency of PEM electrolyzers highlights the system's ability to adapt to varying energy inputs. However, significant challenges in hydrogen storage remain a critical consideration for real-world deployment. Currently, the model utilizes a three-stage compressor for high-pressure storage (up to 200 bar). This method incurs considerable energy penalties and requires large tanks due to hydrogen's low volumetric density of 0.0813 g/L at 25°C and 1 bar. For example, to store the daily output of 15.5 kg of hydrogen at 200 bar, a tank volume of approximately 1 m^3 is necessary, which poses logistical challenges for decentralized applications. Future developments could incorporate advanced storage strategies to improve feasibility. Metal Hydride Materials such as Mg_2Ni or Ti-V-Mn alloys can chemically bind hydrogen at moderate pressures (below 100 bar), achieving storage densities of 80–100 g/L. These systems could utilize waste heat from the waste heat recovery (WHR) unit to release hydrogen, thereby minimizing energy losses (Hu et al., 2023). Cryo-Compressed Storage method which combines high compression (350–700 bar) with cryogenic cooling (−253°C) to enhance density to

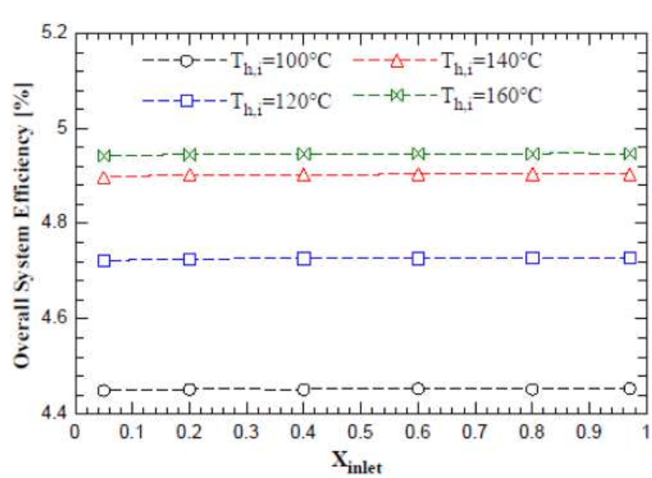

Fig. 10. Overall system efficiency at different steam inlet temperatures.

40–70 g/L. However, liquefaction requires approximately 30 % of hydrogen's energy content, making it more suitable for regions with abundant renewable electricity (Mulky et al., 2024).

6.4. System performance

The overall efficiency of the integrated system shown in Fig. 10, comprising a WHR system (utilizing a 12 ×833 TEG arrangement), an HDH unit, and a PEM electrolyzer, was evaluated at a steam inlet mass flow rate of 10 kg/s under varying steam inlet qualities (0.05–0.97) and temperatures (100°C to 160°C). The 12 × 833 TEG arrangement was determined to generate more power than other configurations, making it the optimal choice for the WHR system. The results indicate that while the overall system efficiency remains relatively constant with changes in steam inlet quality at the same temperature, it increases significantly with rising steam inlet temperatures across all qualities. For example, at 100°C, the overall efficiency remains nearly unchanged as steam inlet quality increases from 0.05 to 0.97, with values ranging from 4.449 % to 4.45 %. However, when the steam inlet temperature is raised to 160°C, the overall efficiency improves, reaching 4.947 % at an inlet quality of 0.97. This increase in efficiency is primarily attributed to enhanced power generation from the WHR system at higher temperatures, which supports higher hydrogen production rates. Supporting this trend, the data reveals that at a steam inlet temperature of 100°C, the maximum heat input to the system rises only slightly from 338.45 kW to 339.28 kW as steam quality increases from 0.05–0.97. Despite the minimal change in heat input, hydrogen production increases with steam quality, while power production decreases slightly. This highlights how the balance between input energy utilization and output parameters influences the overall system efficiency. Specifically, the final efficiency, calculated as the ratio of useful outputs (mass flow rate of hydrogen × HHV + mass flow rate of purified water × h_{fg}) to the maximum heat input ($Q_{max,\ in}$), declines as steam quality increases. This indicates that higher steam quality does not proportionally enhance thermal energy utilization for hydrogen and water production. Overall, the results illustrate that steam inlet temperature plays a more significant role than steam quality in influencing the overall efficiency. The increase in efficiency with rising temperatures underscores the importance of optimizing steam parameters to effectively balance power generation, hydrogen production, and water desalination in the integrated system.

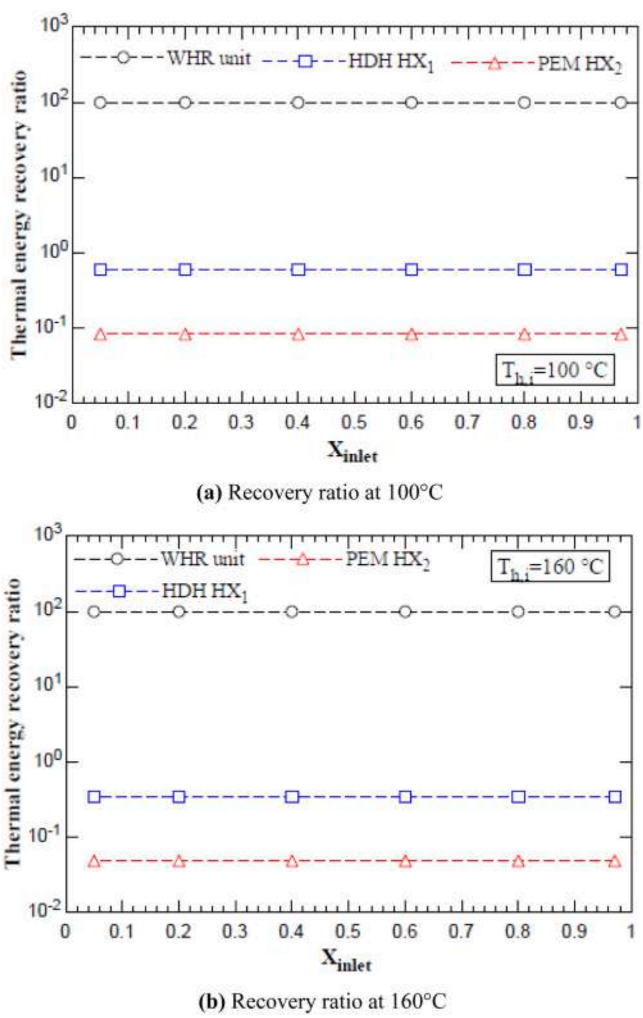

Fig. 11. Thermal energy recovery ratio at steam inlet temperatures.

6.5. Thermal heat recovery

The recovery ratio trends for the integrated WHR, HDH, and PEM systems reveal significant variation with changing steam inlet temperatures. As shown in Figs. 11a and 11b, the recovery ratio (RR) for the WHR system increases with steam inlet temperatures from 100 to 160°C, respectively. This can be attributed to the higher temperature gradient across the TEG units, which enhances power generation efficiency by increasing the thermoelectric effect. As a result, the WHR system can convert a larger portion of the input heat into electricity, with the RR reaching around 99.31 % at 100°C. However, this increase in the WHR recovery ratio comes at the expense of the HDH and PEM units. The RR for the HDH and PEM systems decreases slightly as the inlet temperature increases, indicating that less thermal energy is available for seawater reheating and hydrogen production. This reduction in the recovery ratio for HDH and PEM is tied to the fact that the WHR system extracts more energy from the steam, leaving less heat for the subsequent stages. Thus, while the overall system becomes more effective in electricity generation, the distribution of heat recovery across the subsystems shifts, reflecting the trade-offs inherent in optimizing multi-stage thermal energy recovery systems.

6.6. Control strategy

To enhance the operational stability and adaptability of the proposed integrated system, a structured control strategy is introduced to regulate

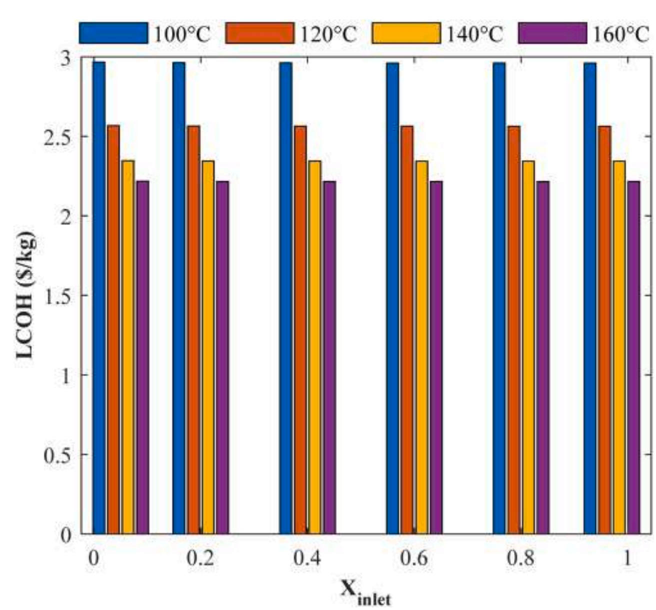

Fig. 12. LCOH as a function of varying waste heat inlet temperatures.

key thermal and flow parameters. The waste heat source, derived from a steam turbine, supplies saturated steam at a constant temperature and quality; however, the **mass flow rate** entering the thermoelectric generator (TEG) heat exchanger can be dynamically adjusted within the range of 2–20 kg/s. A flow control loop is recommended to modulate this parameter in response to the thermal demand of the TEG, thereby optimizing latent heat utilization while mitigating the risks of thermal overloading or underutilization.

On the cooling side, a parallel-flow heat exchanger utilizes water at an inlet temperature of 10 °C and a nominal flow rate of 20 kg/s to maintain an effective temperature gradient across the TEG. A combined flow and temperature regulation system is proposed to ensure adequate heat dissipation and stable electricity generation. Although the freshwater produced by the humidification-dehumidification (HDH) unit is stored and directly supplied to the proton exchange membrane (PEM) electrolyzer without requiring flow regulation, the electricity generated by the waste heat recovery (WHR) system exhibits variability due to changing thermal conditions. To address this, a basic energy management strategy is proposed to synchronize the electrical input to the PEM electrolyzer with the power output of the TEG. This coordination is intended to stabilize hydrogen production, prevent efficiency degradation due to overcurrent, and ensure reliable system performance under dynamic operating conditions.

6.7. Economic analysis

The evaluation of the Levelized Cost of Hydrogen (LCOH) across different steam inlet qualities (0.97–0.05) and temperatures (100 °C to 160 °C), as shown in Fig. 12, highlights a distinct trend: higher waste heat temperatures reduce LCOH, dropping from approximately $2.96/kg at 100 °C to $2.22/kg at 160 °C. While variations in steam quality have a minor impact, a slight increase in LCOH is observed as steam quality decreases, demonstrating the relationship between hydrogen production costs and the efficiency of the waste heat recovery (WHR) system integrated with the Proton Exchange Membrane (PEM) electrolyzer. The decline in LCOH with rising temperatures aligns with thermodynamic principles, where higher temperatures improve thermoelectric generator (TEG) efficiency, leading to higher power output and lower hydrogen production costs. Conversely, at lower temperatures (100–120 °C), the reduced power generation results in higher production costs, with LCOH values above $2.56/kg. While steam quality variations have a relatively small effect, higher steam quality (0.97) consistently yields the lowest LCOH values, increasing slightly as steam quality decreases. The proposed system remains economically competitive compared to market hydrogen prices. Gray hydrogen costs $1.50–$2.50/kg, blue hydrogen ranges from $2.00–$3.50/kg, and green hydrogen is priced between $4.00–$7.00/kg. In Egypt, recent agreements indicate green hydrogen prices of $4.50–$5.00/kg (Ringel et al., 2024). The LCOH values obtained in this study ($2.22–$2.96/kg) remain competitive with blue hydrogen pricing, particularly at higher temperatures (140–160 °C), reinforcing the economic viability of integrating WHR with PEM electrolysis.

The Net Present Value (NPV) analysis for hydrogen production at different selling prices ($2/kg, $3/kg, and $5/kg) provides crucial insights into the system's financial feasibility in Egypt, as illustrated in Fig. 13. Across all scenarios, initial NPVs are negative due to high capital expenditures, transitioning toward profitability as hydrogen sales increase. The break-even period and long-term profitability are strongly influenced by hydrogen price and waste heat temperature.

At $2/kg, the NPV remains negative throughout the 20-year project lifespan, indicating that profitability is unachievable without financial incentives or cost reductions. As shown in Fig. 12, even at 160°C, the NPV remains negative at -$9537.8, while at lower temperatures (100°C), the NPV reaches -$19,136 at Year 20. These results highlight the economic limitations of hydrogen production at low market prices. However, given that gray hydrogen prices in Egypt range from $1.50 to $2.50/kg, government subsidies or carbon credit mechanisms could help bridge this economic gap, making WHR-based hydrogen production more financially viable.

At $3/kg, the system reaches break-even between 10 and 20 years, depending on waste heat temperature. At 100°C, the NPV turns positive at Year 20 ($656.22), while at higher temperatures, profitability is achieved earlier. At 120°C, the project reaches an NPV of $11,945, while at 140°C and 160°C, the final NPVs rise to $23,344 and $34,256, respectively. These values suggest that WHR-driven hydrogen production at $3/kg is financially competitive with blue hydrogen ($2.00–$3.50/kg), particularly at higher operating temperatures where profitability improves significantly.

At $5/kg, the system becomes highly profitable, achieving break-even within 4–5 years. At 100°C, the NPV reaches $40,241 by Year

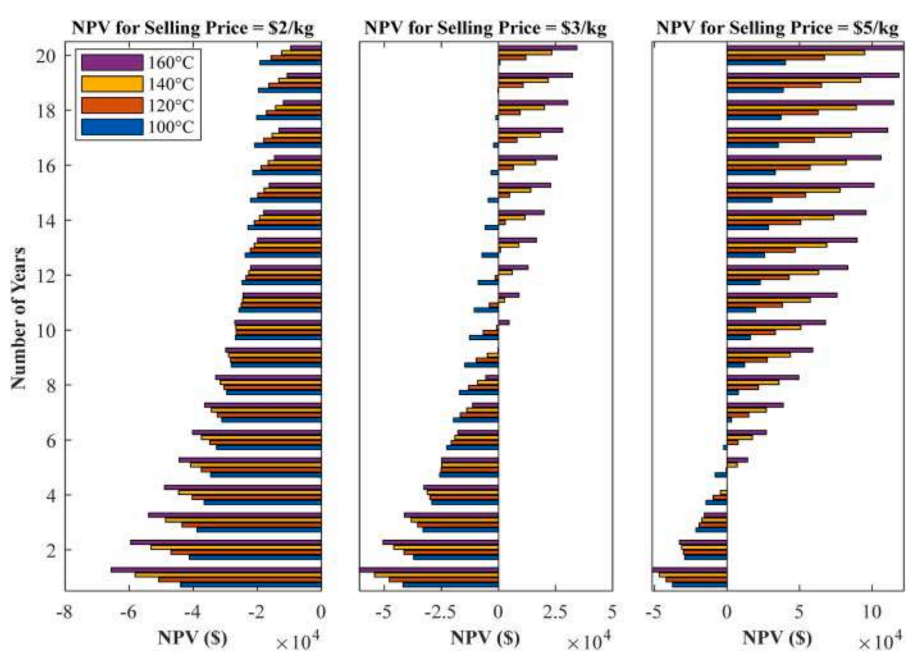

Fig. 13. NPV for different selling prices at different waste heat inlet temperatures.

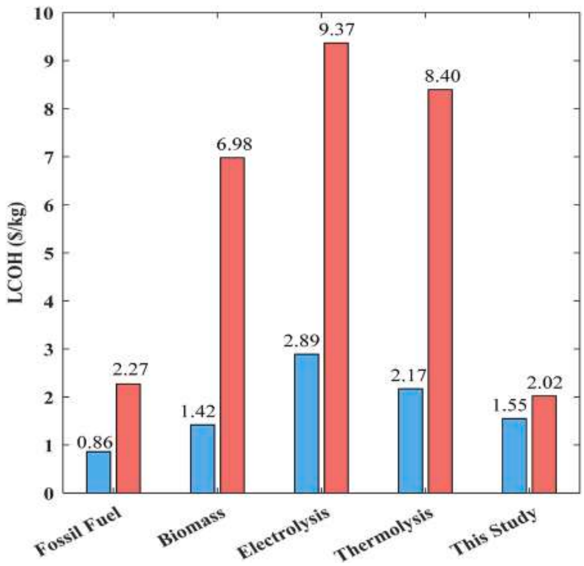

Fig. 14. Minimum and Maximum LCOH Values for Conventional and Alternative Hydrogen Production Pathways.

20. In comparison, at 160°C, it peaks at approximately $121,840, as shown in Fig. 13. These results align with Egypt's current green hydrogen market price of $4.50–$5.00/kg, suggesting that waste heat utilization offers a cost-effective alternative to renewable electrolysis. The high profitability at $5/kg reinforces the system's financial viability, particularly in markets with strong hydrogen demand and carbon pricing mechanisms. Overall, the NPV analysis confirms that hydrogen production from waste heat recovery is financially viable at moderate to high selling prices ($3–$5/kg), with higher waste heat temperatures (140–160°C) ensuring faster break-even and long-term profitability. However, at $2/kg, the project remains unprofitable without external financial support. These findings underscore the importance of market-driven pricing, policy incentives, and carbon credit mechanisms in making WHR-based hydrogen production economically sustainable.

6.8. *Comparative assessment of hydrogen production approaches*

Fig. 14 provides a comparative illustration of minimum and maximum LCOH values across a range of hydrogen production methods, including fossil fuel reforming, biomass conversion, water electrolysis, and thermolysis (El-Emam and Özcan, 2019; Ji and Wang, 2021). While fossil fuel-based methods demonstrate the lowest production cost ($0.86–$2.27/kg), they are environmentally unsustainable. Biomass-based systems span a broader range ($1.42–$6.98/kg), subject to feedstock type and processing efficiency. Water electrolysis, despite being clean, shows the widest and highest LCOH range ($2.89–$9.37/kg), owing to dependence on variable renewable electricity. Although less commercially mature, thermolysis ranges between $2.17–$8.40/kg. In contrast, the current WHR-based system offers a lower-cost, low-emission alternative, positioning itself as a viable candidate for expanding green hydrogen production capacity, especially in industrial settings with abundant low-grade heat. Furthermore, Table 7 presents a detailed comparison between the present study and four notable works in the domain: (Nasser and Hassan, 2023), (Nasser et al., 2024), (Nasser et al., 2022b), and (B. W. Kariuki et al., 2024). These studies span a spectrum of system configurations, including high-grade Rankine cycles, hybrid PV-Wind systems, and PVT-integrated co-production units. The comparison elucidates key distinctions in system architecture, power and hydrogen output, efficiency, and scalability. While systems based on high-temperature waste heat or large-scale renewables show promise, they also present challenges in terms of infrastructure requirements and intermittency. In contrast, the proposed standalone system offers a modular, and cost-effective, with potential for scalable deployment in industries where waste heat is readily available. Overall, this comparative assessment affirms that the integration of WHR with PEM electrolysis represents a strategic pathway for sustainable hydrogen production, balancing cost, environmental responsibility, and adaptability within current energy infrastructures.

The proposed WHR-HDH-PEM system is inherently scalable and accommodates steam flow rates up to 20 kg/s, aligning with lower industrial capacities. The system shows strong potential for large-scale application since industrial steam sources typically range from 50 to 600 kg/s. Its modular design enables linear scalability by replicating WHR-TEG units, ensuring efficient heat recovery and hydrogen production. Increased saline water flow can also enhance HDH and PEM

Table 7
Comparative Overview of Selected Green Hydrogen Production Studies.

Aspect	Present Study	(Nasser and Hassan, 2023)	(Nasser et al., 2024)	(Nasser et al., 2022b)	(B. W. Kariuki et al., 2024)
System Design	TEGs, HDH, PEM electrolyzer (standalone).	Rankine cycle + PEM or SOEC.	PV, PVT, WT, PEM electrolyzer, fuel cell, H_2 storage.	PV, WT, PEM electrolyzer (five PV/WT scenarios).	PVT, PEM electrolyzer, HDH.
Energy Source	Waste heat (100°C–160°C steam).	Cement industry waste heat (360°C–780°C).	Solar and wind	Solar (PV), wind (Egyptian cities).	Solar (PVT, Alexandria, Egypt).
Power Generation	TEGs (36.88 kW) Config 4 at 160 °C	Rankine cycle (steam-based, output not specified).	PV (12 MW), PVT (thermal + electric), WT (variable).	PV/WT combos (variable, scenario-dependent).	PVT (0.123 kW summer, 0.098 kW winter).
Hydrogen Production	15.5 kg/day at 160°C, 0.97 quality.	36.9 kg/hr SOEC 27.4 kg/hr PEM	422 kg/day	3–3.4 kg/day	~0.456–0.36 kg/day
Efficiency (Overall)	4.45 %–4.95 % overall efficiency. PEM 73.65 % at 100°C.	22.91 % max (system-level).	~40 % (energy), 36 % (exergy).	7.97 %–16.23 % (scenario-dependent).	12.77 % summer, 10.11 % winter.
Cost (LCOH)	$2.22–$2.96/kg.	$0.84 - $1.635 /kg	$4.30–$4.88/kg.	$3.67–$4.69/kg.	$5.62/kg summer, $6.62/kg winter.
Feasibility	Standalone, small-scale, HDH freshwater co-benefit.	Industrial-scale cement plant integration.	All-day power via H_2 storage, large-scale renewable focus.	Decentralized, climate-dependent feasibility in Egypt.	Small-scale, coastal application with seasonal adaptability.
Key Parameters	Steam temperature and quality, and TEG configurations.	Rankine fluid, SOEC bleeding ratio (1 % optimal).	Solar irradiance, wind speed, PVT thermal output.	PV/WT ratio, climate conditions	Solar radiation, ambient temp, seasonal variation.
Scalability	Limited by TEG output; modular design.	High via Rankine and industrial heat.	High with renewable integration and storage.	Moderate, depending on PV/WT scaling.	Limited by PVT output; site-specific scalability

performance.

7. Conclusion

Integrating the HDH, WHR, and PEM electrolyzer units into a single system presents a highly efficient and sustainable hydrogen production solution through waste heat recovery and utilization. Steam inlet parameters, particularly temperature and quality, significantly influence the system's thermodynamic performance and electrochemical efficiency, necessitating their optimization to maximize energy recovery and hydrogen yield. The impact of the TEGs units distribution on the system performance is considered. Also, the impact of the waste steam temperature, quality, and mass flow rate is investigated. The following conclusions are obtained.

- Among the investigated configurations, configuration four is identified as the most effective for power generation.
- The system's net power output exhibits a substantial increase from 15.615 kW at 100°C to 36.881 kW at 160°C—an increase of over 130 %. This demonstrates the critical role of elevated steam inlet temperatures in enhancing power generation.
- The system achieves a maximum GOR of 1.892 at a top brine temperature of 53.16°C and freshwater temperature of 37.2°C, contributing to efficient freshwater production in the HDH unit.
- The highest hydrogen production rate, 15.5 kg/day, is observed at a steam inlet temperature of 160°C and a steam quality of 0.97. However, the PEM electrolyzer efficiency decreases from 73.653 % at 100°C to 68.94 % at 160°C, highlighting a trade-off between increased power output and electrolyzer efficiency.
- Overall system efficiency reaches approximately 4.45 % at a steam inlet temperature of 100°C across various steam qualities. As the steam inlet temperature increases to 160°C, the overall system efficiency increases to approximately 4.95 %, reflecting the thermodynamic limitations associated with higher power generation.
- This investigation underscores the importance of balancing steam inlet conditions to optimize the system's energy recovery and hydrogen production capabilities, offering valuable insights into sustainable energy solutions.
- The proposed system not only showcases impressive thermodynamic and electrochemical performance but also demonstrates strong economic and environmental viability. The Levelized Cost of Hydrogen (LCOH) analysis shows that higher waste heat temperatures significantly lower hydrogen production costs $1.55/kg at 160°C, making it competitive with traditional methods.
- Net Present Value (NPV) results indicate that financial feasibility is closely linked to hydrogen prices; higher prices ($3–$5/kg) lead to quicker break-even periods and greater profitability.

Future Work

To build upon the findings of the present study and address the limitations acknowledged during model development and reviewer feedback, the following areas are proposed for future research:

1. Future work will develop a dynamic (transient) model of the integrated WHR-HDH-PEM system to capture real-time behaviors during startup, shutdown, and load fluctuations. This will allow evaluation of system responsiveness, control performance, and thermal inertia under realistic operating conditions.
2. Although the current model operates at 20 kg/s steam flow, industrial applications typically involve flow rates ranging from 50 to 600 kg/s. Future research will focus on modular upscaling strategies, including multi-stream WHR-TEG arrays and expanded HDH-PEM modules, with pilot-scale validation under typical industrial conditions (e.g., 50–100 kg/s).
3. Implementation of adaptive control algorithms is recommended to dynamically manage steam flow, cooling water parameters, and PEM electrolyzer load. A basic feedback-control architecture will be introduced to improve system stability and energy utilization under varying thermal conditions.
4. Future studies will incorporate heat losses from radiation, convection, and conduction in the WHR and HDH systems to improve predictive accuracy and evaluate insulation requirements under industrial deployment.
5. While the current model uses high-pressure compressed storage, future work will assess hybrid systems combining metal hydrides and cryo-compression to reduce footprint and enhance safety. Optimization will consider storage density, energy efficiency, and integration with renewable inputs.

CRediT authorship contribution statement

M.A. Mahmoud: Writing – original draft, Validation, Software, Methodology, Investigation, Formal analysis, Data curation. **Shinsuke Mori:** Supervision. **Sameh Nada:** Supervision. **HASSAN Hamdy:** Writing – review & editing, Visualization, Validation, Methodology, Conceptualization.

Declaration of Competing Interest

We disclose any actual or potential conflict of interest including any financial, personal or other relationships with other people or organizations within three years of beginning the submitted work that could inappropriately influence, or be perceived to influence, this work

Acknowledgments

The authors would like to acknowledge the Mission Department of the Ministry of Higher Education (MOHE) of Egypt for providing a scholarship to conduct this study, as well as the Japan International Cooperation Agency (JICA) for offering some of the facilities, tools, and equipment and the Science, Technology & Development Funding (STDF) department which is sponsoring the research work to conduct this study under granted project No. 51418. Project title: Innovative standalone waste heat recovery system for power generation, freshwater, and hydrogen production and storage.

References

A.M.I.Mohamed, N.A.S.E.-M., 2009. Humidification–dehumidification desalination system driven by geothermal energy. Desalination 249, 602–608.

Abu El-Maaty, A.E., Abdallah, H.K., Ben-Mansour, R., 2024. Performance analysis of a novel two-bed adsorption humidification-dehumidification desalination system using metal-organic framework 801. Energy Convers. Manag 301. https://doi.org/10.1016/j.enconman.2023.118020.

Ahiska, R., Mamur, H., 2013. Design and implementation of a new portable thermoelectric generator for low geothermal temperatures. IET Renew. Power Gener. 7, 700–706. https://doi.org/10.1049/iet-rpg.2012.0320.

Ahmed, H.A., Megahed, T.F., Mori, S., Nada, S., Hassan, H., 2023. Novel design of thermo-electric air conditioning system integrated with PV panel for electric vehicles: performance evaluation. Appl. Energy 349, 121662. https://doi.org/10.1016/j.apenergy.2023.121662.

Alirahmi, S.M., Rostami, M., Farajollahi, A.H., 2020. Multi-criteria design optimization and thermodynamic analysis of a novel multi-generation energy system for hydrogen, cooling, heating, power, and freshwater. Int. J. Hydrog. Energy 45, 15047–15062. https://doi.org/10.1016/j.ijhydene.2020.03.235.

bchoate, n.d. Waste Heat Recovery: Technology and Opportunities in U.S. Industry.

Bergman, T.L., Lavine, A.S., Incropera, F.P., DeWitt, D.P., 2018. Fundamentals of Heat and Mass Transfer, 8th Edition, 8th ed. Wiley.

Chen, M., Rosendahl, L.A., Condra, T., 2011. A three-dimensional numerical model of thermoelectric generators in fluid power systems. Int. J. Heat. Mass Transf. 54, 345–355. https://doi.org/10.1016/j.ijheatmasstransfer.2010.08.024.

Contreras Bilbao, D., 2021. Valorization of the waste heat given off in a system alkaline electrolyzer-photovoltaic array to improve hydrogen production performance: case study Antofagasta, Chile. Int. J. Hydrog. Energy 46, 31108–31121. https://doi.org/10.1016/j.ijhydene.2021.07.016.

Dave, T., Krishnan, S., 2021. Performance evaluation and characterization of a direct absorption solar humidifier for humidification-dehumidification desalination. J. Sol. Energy Eng. Trans. ASME 143. https://doi.org/10.1115/1.4047670.
Dehwah, A.H.A., Asif, M., Budaiwi, I.M., Alshibani, A., 2020. Techno-economic assessment of rooftop PV systems in residential buildings in hot–humid climates. Sustain 12, 1–19. https://doi.org/10.3390/su122310060.
Dincer, I., Acar, C., 2014. Review and evaluation of hydrogen production methods for better sustainability. Int. J. Hydrog. Energy 40, 11094–11111. https://doi.org/10.1016/j.ijhydene.2014.12.035.
Ding, Q., Alotaibi, M.A., Lui, C., 2025. Sustainable process modeling and holistic 4E assessment of an innovative CHP plant with renewable hydrogen production based on multi-heat recovery and PEM electrolyzer. Process Saf. Environ. Prot. 194, 730–751. https://doi.org/10.1016/J.PSEP.2024.12.038.
Egypt., C.B.O., 2025. Central Bank Of Egypt. [WWW Document]. URL https://www.cbe.org.eg/en/.
El-Emam, R.S., Özcan, H., 2019. Comprehensive review on the techno-economics of sustainable large-scale clean hydrogen production. J. Clean. Prod. 220, 593–609. https://doi.org/10.1016/j.jclepro.2019.01.309.
ENERGY, T.S., 2025. Costs of cryogenic air separation - Thunder Said Energy [WWW Document]. URL https://thundersaidenergy.com/.
Energy Systems, 2023. Clim. Chang. 2022 - Mitig. Clim. Chang. 613–746. https://doi.org/10.1017/9781009157926.008.
G. Basiony, M., Nada, S., Mori, S., Hassan, H., 2024. Performance evaluation of standalone new solar energy system of hybrid PV/electrolyzer/fuel cell/MED-MVC with hydrogen production and storage for power and freshwater building demand. Int. J. Hydrog. Energy 77, 1217–1234. https://doi.org/10.1016/j.ijhydene.2024.06.211.
Garg, K., Khullar, V., Das, S.K., Tyagi, H., 2018. Numerical Study of Nanofluid-Based Solar Collector for Humidification-Dehumidification (HDH) Desalination. https://doi.org/10.1115/IMECE2018-87318.
Garg, K., Das, S.K., Tyagi, H., 2022. Thermal design of a humidification-dehumidification desalination cycle consisting of packed-bed humidifier and finned-tube dehumidifier. Int. J. Heat. Mass Transf. 183. https://doi.org/10.1016/j.ijheatmasstransfer.2021.122153.
Giakoumakis, G., Sidiras, D., 2025. Production and Storage of Hydrogen from Biomass and Other Sources: Technologies and Policies, 18, 650 Energies 2025 18, 650. https://doi.org/10.3390/EN18030650.
Glenk, G., Reichelstein, S., 2019. Economics of converting renewable power to hydrogen. Nat. Energy 2019 43 (4), 216–222. https://doi.org/10.1038/s41560-019-0326-1.
Gurau, V., Barbir, F., Liu, H., 2000. An analytical solution of a half-cell model for PEM fuel cells. J. Electrochem. Soc. 147, 2468. https://doi.org/10.1149/1.1393555.
Hewawasam, L.S., Jayasena, A.S., Afnan, M.M.M., Ranasinghe, R.A.C.P., Wijewardane, M.A., 2020. Waste heat recovery from thermo-electric generators (TEGs). Energy Rep. 6, 474–479. https://doi.org/10.1016/j.egyr.2019.11.105.
Holmgren, M., 2024. X Steam, Thermodynamic properties of water and steam.
Hsiao, Y.Y., Chang, W.C., Chen, S.L., 2010. A mathematic model of thermoelectric module with applications on waste heat recovery from automobile engine. Energy 35, 1447–1454. https://doi.org/10.1016/j.energy.2009.11.030.
Hu, J., Wang, W., Xie, L., Sun, G., Shen, H., Li, X., Li, P., Zhang, J., Zu, X., Xiao, H., 2023. Effects of NH4+ doping on the hydrogen storage properties of metal hydrides. Int. J. Hydrog. Energy 48, 19153–19159. https://doi.org/10.1016/J.IJHYDENE.2023.01.348.
Hyland, R.W., Wexler, A., 1983. Formulations for the thermodynamic properties of dry air from 173. 15k To 473. 15k, and of saturated moist air from 173. 15K TO 372. 15K, AT PRESSURES TO 5 MPa. ASHRAE Trans. 89, 520–535.
Ji, M., Wang, J., 2021. Review and comparison of various hydrogen production methods based on costs and life cycle impact assessment indicators. Int. J. Hydrog. Energy 46, 38612–38635. https://doi.org/10.1016/j.ijhydene.2021.09.142.
Jouhara, H., Almahmoud, S., Chauhan, A., Delpech, B., Bianchi, G., Tassou, S.A., Llera, R., Lago, F., Arribas, J.J., 2017. Experimental and theoretical investigation of a flat heat pipe heat exchanger for waste heat recovery in the steel industry. Energy 141, 1928–1939. https://doi.org/10.1016/j.energy.2017.10.142.
Kahani, M., Zamen, M., Ahmadi, M.H., Sadri, S., 2024. Technoeconomic assessment of indirect-contact HDH desalination unit driven by boiler blowdown of steam power plant. Energy Sci. Eng. 12, 3437–3452. https://doi.org/10.1002/ese3.1827.
Kariuki, B., Hassan, H., Ahmed, M., Ookawara, S., Emam, M., 2024. Seasonal thermo-enviro-economic performance analyses of concentrated PV/T integrated with humidification-dehumidification water desalination system. Appl. Therm. Eng. 248, 123331. https://doi.org/10.1016/j.applthermaleng.2024.123331.
Kariuki, B.W., Emam, M., Ookawara, S., Hassan, H., 2024. New hybrid system of PV/T, solar collectors, PEM electrolyzer, and HDH for hydrogen and freshwater production: Seasonal performance investigation. Energy 312, 133553. https://doi.org/10.1016/j.energy.2024.133553.
Khalil, H., Hassan, H., 2019. Enhancement thermoelectric generators output power from heat recovery of chimneys by using flaps. J. Power Sources 443, 227266. https://doi.org/10.1016/j.jpowsour.2019.227266.
Khalil, H., Hassan, H., 2020. Enhancement of waste heat recovery from vertical chimney via thermoelectric generators by heat spreader. Process Saf. Environ. Prot. 140, 314–329. https://doi.org/10.1016/j.psep.2020.05.023.
khanmohammadi, S., Saadat-Targhi, M., 2019. Performance enhancement of an integrated system with solar flat plate collector for hydrogen production using waste heat recovery. Energy 171, 1066–1076. https://doi.org/10.1016/J.ENERGY.2019.01.096.
Khater, A.M., Soliman, A., Ahmed, T.S., Ismail, I.M., 2021. Power generation in white cement plants from waste heat recovery using steam-organic combined Rankine cycle. Case Stud. Chem. Environ. Eng. 4, 100138. https://doi.org/10.1016/j.cscee.2021.100138.
Lesage, F.J., Sempels, É .V., Lalande-Bertrand, N., 2013. A study on heat transfer enhancement using flow channel inserts for thermoelectric power generation. Energy Convers. Manag 75, 532–541. https://doi.org/10.1016/j.enconman.2013.07.002.
Ma, H.K., Lin, C.P., Wu, H.P., Peng, C.H., Hsu, C.C., 2015. Waste heat recovery using a thermoelectric power generation system in a biomass gasifier. Appl. Therm. Eng. 88, 274–279. https://doi.org/10.1016/j.applthermaleng.2014.09.070.
Manzotti, A., Quattrocchi, E., Curcio, A., Kwok, S.C.T., Santarelli, M., Ciucci, F., 2022. Membraneless electrolyzers for the production of low-cost, high-purity green hydrogen: a techno-economic analysis. Energy Convers. Manag 254, 115156. https://doi.org/10.1016/j.enconman.2021.115156.
Mohammadi, A., Mehrpooya, M., 2019. Thermodynamic and economic analyses of hydrogen production system using high temperature solid oxide electrolyzer integrated with parabolic trough collector. J. Clean. Prod. 212, 713–726. https://doi.org/10.1016/j.jclepro.2018.11.261.
Møller, K.T., Jensen, T.R., Akiba, E., Li, H. wen, 2017. Hydrogen - a sustainable energy carrier. Prog. Nat. Sci. Mater. Int. 27, 34–40. https://doi.org/10.1016/j.pnsc.2016.12.014.
Mulky, L., Srivastava, S., Lakshmi, T., Sandadi, E.R., Gour, S., Thomas, N.A., Shanmuga Priya, S., Sudhakar, K., 2024. An overview of hydrogen storage technologies – Key challenges and opportunities. Mater. Chem. Phys. 325, 129710. https://doi.org/10.1016/J.MATCHEMPHYS.2024.129710.
Nami, H., Akrami, E., Ranjbar, F., 2017. Hydrogen production using the waste heat of Benchmark pressurized Molten carbonate fuel cell system via combination of organic Rankine cycle and proton exchange membrane (PEM) electrolysis. Appl. Therm. Eng. 114, 631–638 https://doi.org/10.1016/J.Appl Ehermal Eng.2016.12.018.
Nasser, M., Hassan, H., 2023. Assessment of hydrogen production from waste heat using hybrid systems of Rankine cycle with proton exchange membrane/solid oxide electrolyzer. Int. J. Hydrog. Energy 48, 7135–7153. https://doi.org/10.1016/j.ijhydene.2022.11.187.
Nasser, M., Megahed, T.F., Ookawara, S., Hassan, H., 2022b. Techno-economic assessment of clean hydrogen production and storage using hybrid renewable energy system of PV/Wind under different climatic conditions. Sustain. Energy Technol. Assess. 52, 102195. https://doi.org/10.1016/j.seta.2022.102195.
Nasser, M., Megahed, T.F., Ookawara, S., Hassan, H., 2022a. A review of water electrolysis–based systems for hydrogen production using hybrid/solar/wind energy systems. Environ. Sci. Pollut. Res. 1, 1–25. https://doi.org/10.1007/S11356-022-23323-Y.
Nasser, M., Awad, M.M., Hassan, A.A., 2024. 4E assessment of all-day clean electricity generation systems based on green hydrogen integrated system using PV and PVT solar collectors and wind turbines. Int. J. Hydrogen Energy. https://doi.org/10.1016/j.ijhydene.2024.05.089.
Ni, M., Leung, M.K.H., Leung, D.Y.C., 2008. Energy and exergy analysis of hydrogen production by a proton exchange membrane (PEM) electrolyzer plant. Energy Convers. Manag 49, 2748–2756. https://doi.org/10.1016/j.enconman.2008.03.018.
Niu, X., Yu, J., Wang, S., 2009. Experimental study on low-temperature waste heat thermoelectric generator. J. Power Sources 188, 621–626. https://doi.org/10.1016/j.jpowsour.2008.12.067.
Noor, W.Bin, Amin, T., 2024. Towards sustainable energy: a comprehensive review on hydrogen integration in renewable energy systems. Futur. Energy 3, 1–17. https://doi.org/10.55670/fpll.fuen.3.4.1.
Nurizat Rahman, M., Abdul Wahid, M., 2024. Green hydrogen prospects in Peninsular Malaysia: a techno-economic analysis via Monte Carlo simulations. Futur. Sustain 2, 27–45. https://doi.org/10.55670/fpll.fusus.2.2.4.
Olabi, A.G., Al-Murisi, M., Maghrabie, H.M., Yousef, B.A., Sayed, E.T., Alami, A.H., Abdelkareem, M.A., 2022. Potential applications of thermoelectric generators (TEGs) in various waste heat recovery systems. Int. J. Thermofluids 16. https://doi.org/10.1016/j.ijft.2022.100249.
Ononogbo, C., Nwosu, E.C., Nwakuba, N.R., Nwaji, G.N., Nwufo, O.C., Chukwuezie, O. C., Chukwu, M.M., Anyanwu, E.E., 2023. Opportunities of waste heat recovery from various sources: Review of technologies and implementation. Heliyon 9, e13590. https://doi.org/10.1016/j.heliyon.2023.e13590.
Ozcan, H., Dincer, I., 2017. Energy and exergy analyses of a solar based hydrogen production and compression system. Int. J. Hydrog. Energy 42, 21414–21428. https://doi.org/10.1016/j.ijhydene.2017.05.001.
Peterson, G.P., Fletcher, L.S., 1988. Evaluation of Thermal Contact Conductance Between Mold Compound and Heat Spreader Materials.
Prakash Narayan, G., Mistry, K.H., Sharqawy, M.H., Zubair, S.M., Lienhard, J.H., 2010. Energy effectiveness of simultaneous heat and mass exchange devices. Front. Heat. Mass Transf. 1. https://doi.org/10.5098/hmt.v1.2.3001.
Prakash Narayan, G., St. John, M.G., Zubair, S.M., Lienhard, J.H., 2013. Thermal design of the humidification dehumidification desalination system: An experimental investigation. Int. J. Heat. Mass Transf. 58, 740–748. https://doi.org/10.1016/j.ijheatmasstransfer.2012.11.035.
Pujol, T., T'Jollyn, I., Massaguer, E., Massaguer, A., Cózar, I.R., De Paepe, M., 2023. Design optimization of plate-fin heat sink with forced convection for single-module thermoelectric generator. Appl. Therm. Eng. 221. https://doi.org/10.1016/j.applthermaleng.2022.119866.
Razmi, A.R., Alirahmi, S.M., Nabat, M.H., Assareh, E., Shahbakhti, M., 2022. A green hydrogen energy storage concept based on parabolic trough collector and proton exchange membrane electrolyzer/fuel cell: Thermodynamic and exergoeconomic analyses with multi-objective optimization. Int. J. Hydrog. Energy 47, 26468–26489. https://doi.org/10.1016/J.IJHYDENE.2022.03.021.

Rezaei, M., Naghdi-Khozani, N., Jafari, N., 2020. Wind energy utilization for hydrogen production in an underdeveloped country: An economic investigation. Renew. Energy 147, 1044–1057. https://doi.org/10.1016/j.renene.2019.09.079.

Rezania, A., Rosendahl, L.A., Andreasen, S.J., 2012. Experimental investigation of thermoelectric power generation versus coolant pumping power in a microchannel heat sink. Int. Commun. Heat. Mass Transf. 39, 1054–1058. https://doi.org/10.1016/j.icheatmasstransfer.2012.07.010.

Ringel, M., Stöckigt, G., Shamon, H., Vögele, S., 2024. Green hydrogen cooperation between Egypt and Europe: The perspective of locals in Suez and Port Said. Int. J. Hydrog. Energy 79, 1501–1510. https://doi.org/10.1016/j.ijhydene.2024.06.239.

Rowe, D.M., Bhandari, C.M., 1983. Modern Thermoelectrics, Holt technology. Holt, Rinehart and Winston.

Rowe, D.M., Min, G., 1998. Evaluation of thermoelectric modules for power generation, Journal of Power Sources.

S. Farsad, A.B., 2011. Analysis of a solar desalination unit with humidification–dehumidification cycle using DoE method. Desalination 278, 70–76.

Sasaki, K., Horikawa, D., Goto, K., 2014. Consideration of Thermoelectric Power Generation by Using Hot Spring Thermal Energy or Industrial Waste Heat. J. Electron. Mater. 44, 391–398.

Shah, M.M., 1979. A GENERAL CORRELATION FOR HEAT TRANSFER DURING FILM CONDENSATION INSIDE PIPES. Int. J. Heat. Mass Transf. 22, 547–556.

Sharqawy, M.H., Lienhard, J.H., Zubair, S.M., 2010. Thermophysical properties of seawater: a review of existing correlations and data. Desalin. Water Treat. 16, 354–380. https://doi.org/10.5004/dwt.2010.1079.

Sharqawy, M.H., Antar, M.A., Zubair, S.M., Elbashir, A.M., 2014. Optimum thermal design of humidification dehumidification desalination systems. Desalination. https://doi.org/10.1016/j.desal.2014.06.016.

Shiva Kumar, S., Lim, H., 2022. An overview of water electrolysis technologies for green hydrogen production. Energy Rep. 8, 13793–13813. https://doi.org/10.1016/j.egyr.2022.10.127.

Sievers, M., Lienhard V, J.H., 2015. Design of plate-fin tube dehumidifiers for humidification-dehumidification desalination systems. Heat. Transf. Eng. 36, 223–243. https://doi.org/10.1080/01457632.2014.916153.

Tzimas, E., Filiou, C., Peteves, S.D., Veyret, J., 2003. Hydrogen Storage: State-of-the-Art and Future Perspective, European Commission.

Wang, F., Wang, L., Zhang, H., Xia, L., Miao, H., Yuan, J., 2021. Design and optimization of hydrogen production by solid oxide electrolyzer with marine engine waste heat recovery and ORC cycle. Energy Convers. Manag 229, 113775. https://doi.org/10.1016/j.enconman.2020.113775.

Yang, Z., Pradogonjal, J., Phillips, M., Lan, S., Powell, A., Vaqueiro, P., Gao, M., Stobart, R., Chen, R., 2017. Improved Thermoelectric Generator Performance Using High Temperature Thermoelectric Materials. SAE Tech. Pap. 2017-March. https://doi.org/10.4271/2017-01-0121.

Yavuz, H., 2020. Modelling and simulation of a heaving wave energy converter based PEM hydrogen generation and storage system. Int. J. Hydrog. Energy 45, 26413–26425. https://doi.org/10.1016/j.ijhydene.2020.06.099.

Zarabi Golkhatmi, S., Asghar, M.I., Lund, P.D., 2022. A review on solid oxide fuel cell durability: latest progress, mechanisms, and study tools. Renew. Sustain. Energy Rev. 161, 112339. https://doi.org/10.1016/J.RSER.2022.112339.